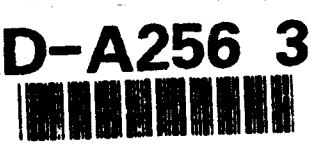

(2)

NAVAL POSTGRADUATE SCHOOL
Monterey, California

THESIS

Kink-Assisted Mode Hopping
in a Surface Wave Resonator

by

Charles B. McClelland

June, 1992

Co-Advisor — Bruce Denardo
Co-Advisor — Andrés Larraza

Approved for Public Release; distribution is unlimited.

Unclassified

CURITY CLASSIFICATION OF THIS PAGE

REPORT DOCUMENTATION PAGE

Form Approved
OMB No. 0704-0188

a REPORT SECURITY CLASSIFICATION NCLASSIFIED	1b RESTRICTIVE MARKINGS
a SECURITY CLASSIFICATION AUTHORITY	3 DISTRIBUTION/AVAILABILITY OF REPORT Approved for public release; distribution is unlimited.
b DECLASSIFICATION/DOWNGRADING SCHEDULE	
PERFORMING ORGANIZATION REPORT NUMBER(S)	5 MONITORING ORGANIZATION REPORT NUMBER(S)
a NAME OF PERFORMING ORGANIZATION aval Postgraduate School	6b OFFICE SYMBOL (If applicable) 33
7a NAME OF MONITORING ORGANIZATION Naval Postgraduate School
c ADDRESS (City, State, and ZIP Code) onterey, CA 93943-5000	7b ADDRESS (City, State, and ZIP Code) Monterey, CA 93943-5000
a NAME OF FUNDING/SPONSORING ORGANIZATION	8b OFFICE SYMBOL (If applicable)
9 PROCUREMENT INSTRUMENT IDENTIFICATION NUMBER
c ADDRESS (City, State, and ZIP Code)	10 SOURCE OF FUNDING NUMBERS

PROGRAM ELEMENT NO	PROJECT NO	TASK NO	WORK UNIT ACCESSION NO.

1 TITLE (Include Security Classification)

INK-ASSISTED MODE HOPPING IN A SURFACE WAVE RESONATOR

2 PERSONAL AUTHOR(S)

cClelland, Charles B.

3a TYPE OF REPORT	13b TIME COVERED	14 DATE OF REPORT (Year, Month, Day)	15 PAGE COUNT
asters Thesis	FROM _____ TO _____	June 1992	68

6 SUPPLEMENTARY NOTATION The views expressed in this thesis are those of the author and do not eflect the official policy or position of the Department of Defense or the U. S. overnment.

7 COSATI CODES			18 SUBJECT TERMS (Continue on reverse if necessary and identify by block number)
FIELD	GROUP	SUB-GROUP	Kink, Soliton; mode-hopping, surface wave, resonator

9 ABSTRACT (Continue on reverse if necessary and identify by block number)

Self-localized kink structures have been observed in standing surface gravity waves in a parametrically driven annular channel of liquid. The kink regions have substantially greater amplitude and smaller wavelength than the extended mode region, and can exist indefinitely only for sufficiently large drive levels such that the structures exhibit violent breaking and jetting motion. For lower drive levels, the structures exist as transients that spontaneously participate in the transition from one mode to a mode with either one less or one more wavelength. In this mode hopping process, the destruction or creation of the wavelength occurs in the kink region. The kink structures are predicted to exist according to a theory that simultaneously allows amplitude *and* wave number modulations of a finite-amplitude standing wave. This situation is in fundamental contrast to nonlinear Schrödinger solitons, which correspond to only amplitude modulations, and to all other known types of solitons.

0 DISTRIBUTION/AVAILABILITY OF ABSTRACT	21 ABSTRACT SECURITY CLASSIFICATION	
☐ UNCLASSIFIED/UNLIMITED ☐ SAME AS RPT ☐ DTIC USERS	Unclassified	
2a NAME OF RESPONSIBLE INDIVIDUAL ruce Denardo	22b TELEPHONE (Include Area Code) 408-646-3485	22c OFFICE SYMBOL PH/De

) Form 1473, JUN 86 Previous editions are obsolete. SECURITY CLASSIFICATION OF THIS PAGE

S/N 0102-LF-014-6603 Unclassified

Approved for Public Release; distribution is unlimited.

Kink-Assisted Mode Hopping in a Surface Wave Resonator

by

Charles B. McClelland
Captain, United States Marine Corps
B.S., United States Naval Academy, 1986

Submitted in partial fulfillment
of the requirements for the degree of

MASTER OF SCIENCE IN PHYSICS

from the

NAVAL POSTGRADUATE SCHOOL
June 1992

Author: _____
Charles B. McClelland

Approved By: _____
Bruce C. Denardo, Thesis Co-Advisor

_____
Andrés Larraza, Thesis Co-Advisor

_____
Karlheinz Woehler, Second Reader

_____
Karlheinz Woehler, Physics Department Chairman

ABSTRACT

Self-localized kink structures have been observed in standing surface gravity waves in a parametrically driven annular channel of liquid. The kink regions have substantially greater amplitude and smaller wavelength than the extended mode region, and can exist indefinitely only for sufficiently large drive levels such that the structures exhibit violent breaking and jetting motion. For lower drive levels, the structures exist as transients that spontaneously participate in the transition from one mode to a mode with either one less or one more wavelength. In this mode hopping process, the destruction or creation of the wavelength occurs in the kink region. The kink structures are predicted to exist according to a theory that simultaneously allows amplitude *and* wave number modulations of a finite-amplitude standing wave. This situation is in fundamental contrast to nonlinear Schrödinger solitons, which correspond to only amplitude modulations, and to all other known types of solitons.

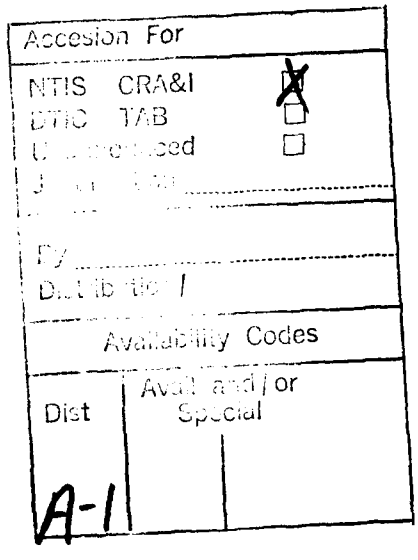

TABLE OF CONTENTS

I. INTRODUCTION

Far off equilibrium systems can exhibit behavior that is fundamentally different from that in the near-equilibrium limit. Examples are shock waves, solitons (discussed below), chaos, and turbulence. We have observed new dramatic behavior in a system driven far from equilibrium. In our experiment, steady-state standing waves are maintained on the surface of a liquid in a vertically oscillated annular channel. If the drive frequency is slowly and monotonically changed, and the drive amplitude is sufficiently large, the transition to the next mode is accompanied by the spontaneous formation of a localized kink structure (Fig. I.1). The kink can appear at any location around the annulus, and dies out as the transition is completed. It is in the kink structure that the creation of one wavelength occurs in the case of up-hopping, or the annihilation of one wavelength in the case of down-hopping. This kink-assisted mode hopping, which we have investigated both experimentally and theoretically, is the subject of this thesis.

In systems that are locally (as opposed to globally) driven, there is a simple transition from one mode to another as the drive frequency is slowly changed: nodes continuously emerge from or disappear into the drive location. This occurs, for example, in sound waves driven by a loudspeaker at one end of a cylinder. For systems that are weakly globally driven, the transitions are even simpler: between the modes there are frequency gaps in which no excitation occurs. However, the situation is fundamentally different for systems that are globally driven far from equilibrium. In this case there is hopping at finite amplitude from one mode to another, and it is an interesting question how a wavelength is created or annihilated in the process.

An important occurrence of mode hopping is in semiconductor diode lasers. As the temperature or current (analogous to our drive frequency or amplitude, respectively) is changed, the frequency can hysteretically jump to a different value. More important in these systems is that mode hopping evidently plays a role in partition noise, which is a result of the excitation of different modes whose amplitudes vary in time (Weidel and Petermann, 1981). This effect is not restricted to multimode lasers, but can also occur in some "single"-frequency lasers operated at high current levels. An understanding of the dynamics of mode hopping may thus lead to the manufacture of diode lasers with reduced noise characteristics.

We believe that the nature of the mode hopping in the surface wave resonator is a general phenomenon which may occur in a variety of systems, including diode lasers (although this connection has not yet been established). Indeed, as explained in Sec. IV.B, we have observed similar behavior in the mode hopping of computer-simulated waves on a string. The surface wave resonator could thus be an accessible system with regard to transient behavior that is difficult or impossible to directly observe in other systems.

The discovery of the kink-assisted mode hopping was a result of ongoing investigations of *solitons*, which are exponentially localized waves of constant shape in dispersive systems. In such a wave there is a stable balance between nonlinearity, which tends to cause the wave to shock, and dispersion, which tends to cause the wave to spread (because components of different wavelength travel at different speeds). Solitons were first observed as surface waves in a canal in 1834, and are planned to be employed this decade as optical waves in transoceanic fiber telecommunications (Mollenauer *et al.*, 1991). Solitons may

also play a role in energy and information transfer in some biological systems (Davydov, 1985). The fiber optic and Davydov solitons are of the nonlinear Schrödinger (NLS) type.

An example of a soliton is a standing localized surface wave observed in a long uniform channel of deep liquid (Wu *et al.*, 1984). Steady-state motion is achieved by vertically oscillating the channel. In the frame of reference of the channel, the liquid is motionless except in a relatively small region where it sloshes transverse to the channel (Fig. I.2a). The state is referred to as a *breather.* The underlying approximate description was found to be an NLS equation (Larraza and Putterman, 1984), which describes these states as amplitude modulations of the cutoff mode (in which the liquid sloshes transversely with uniform amplitude). The breather can be understood as a self-trapped state which can occur because the oscillations soften, i.e., the resonance frequency decreases for greater response amplitudes. The oscillations harden for a sufficiently shallow liquid, and consequently a *cutoff kink* soliton can exist (Denardo *et al.*, 1990). In this state, the liquid sloshes at constant amplitude transverse to the channel in two extended regions, with a 180^{o} phase difference (Fig. I.2b). The kink is the localized transition that connects the motion in the two regions. The observations showed that the surface wave kink can exist at amplitudes substantially beyond which the perturbation theory is valid, indicating that the state is a more general phenomenon than the theory predicts.

Experiments with a mechanical lattice yielded analogous breather and kink solitons and, more importantly, fundamentally new types of localized states (Denardo *et al.*, 1992a). These are *domain walls,* which are localized transition

regions that connect two standing wave regions of different wave number, and *noncutoff kinks*, which connect two standing wave regions of the same wave number with a difference in spatial phase (Fig. I.3). Neither the NLS equation nor any other known modulational equation describes these new states. An understanding of the states may thus lead to new solitons. Theoretical progress has recently been made by considering the states as modulations in both amplitude and wave number (Denardo *et al.*, 1992b).

The kink-assisted mode hopping was discovered accidentally while we were attempting to obtain a steady-state noncutoff kink in a surface wave resonator. A theoretical investigation (Ch. II) had predicted such a solution as a continuum analog of the lattice noncutoff kink. Although we were eventually able to obtain a permanent kink, we also observed that the kink participated in mode hopping.

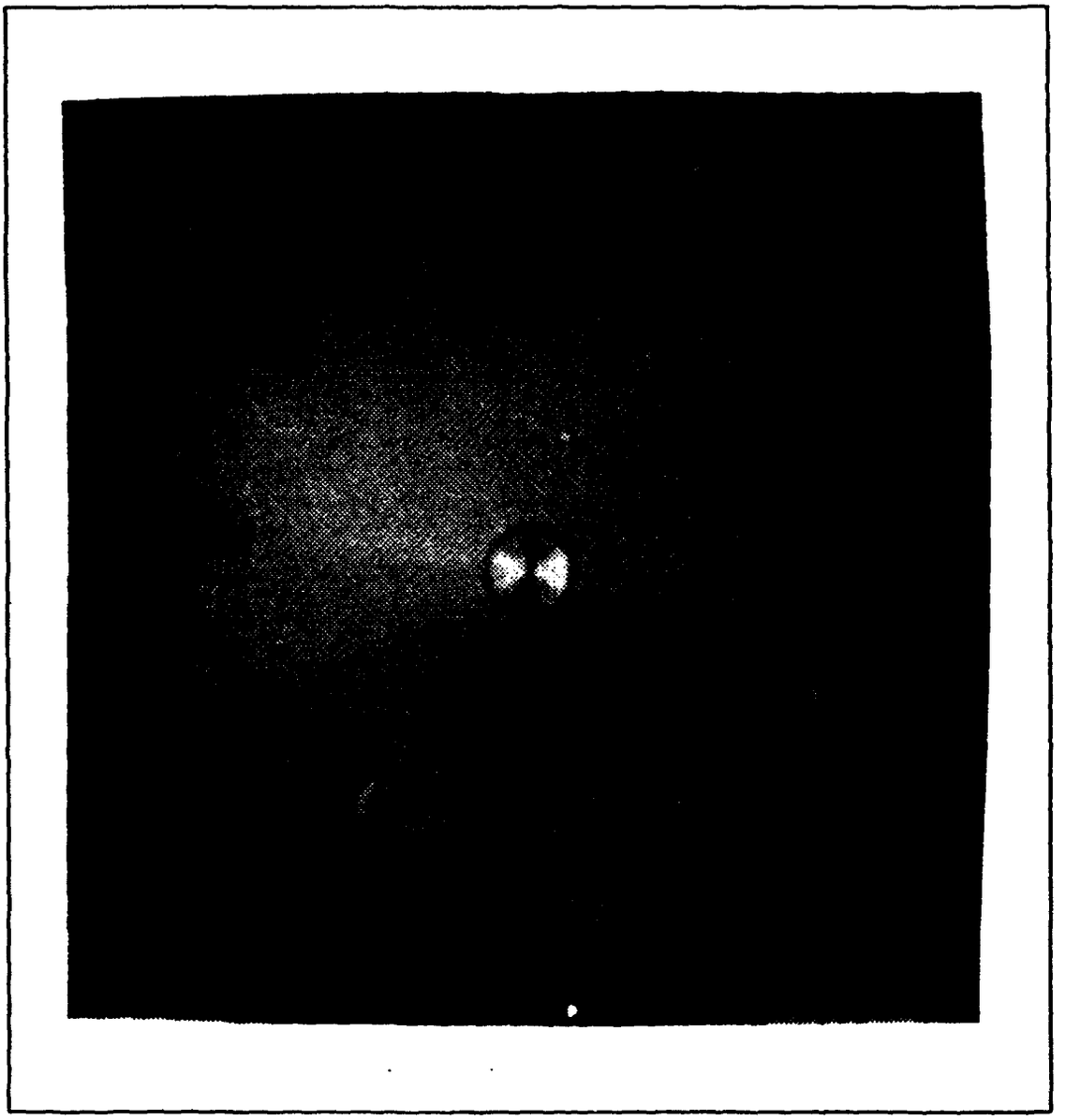

Fig. I.1. Frame-grabbed image of the observed vertical displacement of the surface during mode hopping in an annular channel of liquid. This image is projected on a conical mirror so that the vertical displacement of the free surface is represented radially.

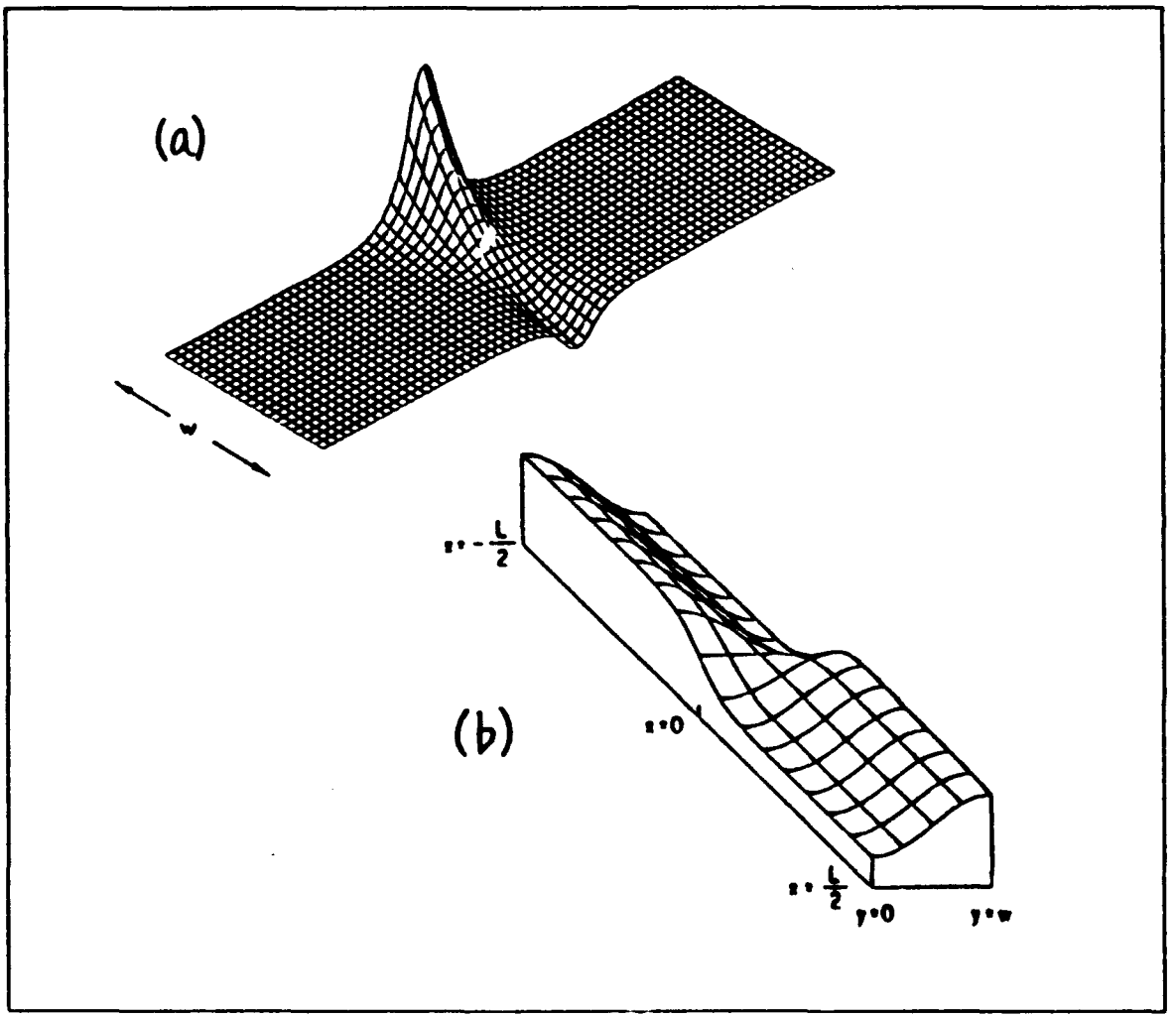

Fig. I.2. Steady-state solitons on the surface of a liquid in a channel: (a) breather soliton, in the case of deep liquid, and (b) cutoff kink soliton, in the case of shallow liquid.

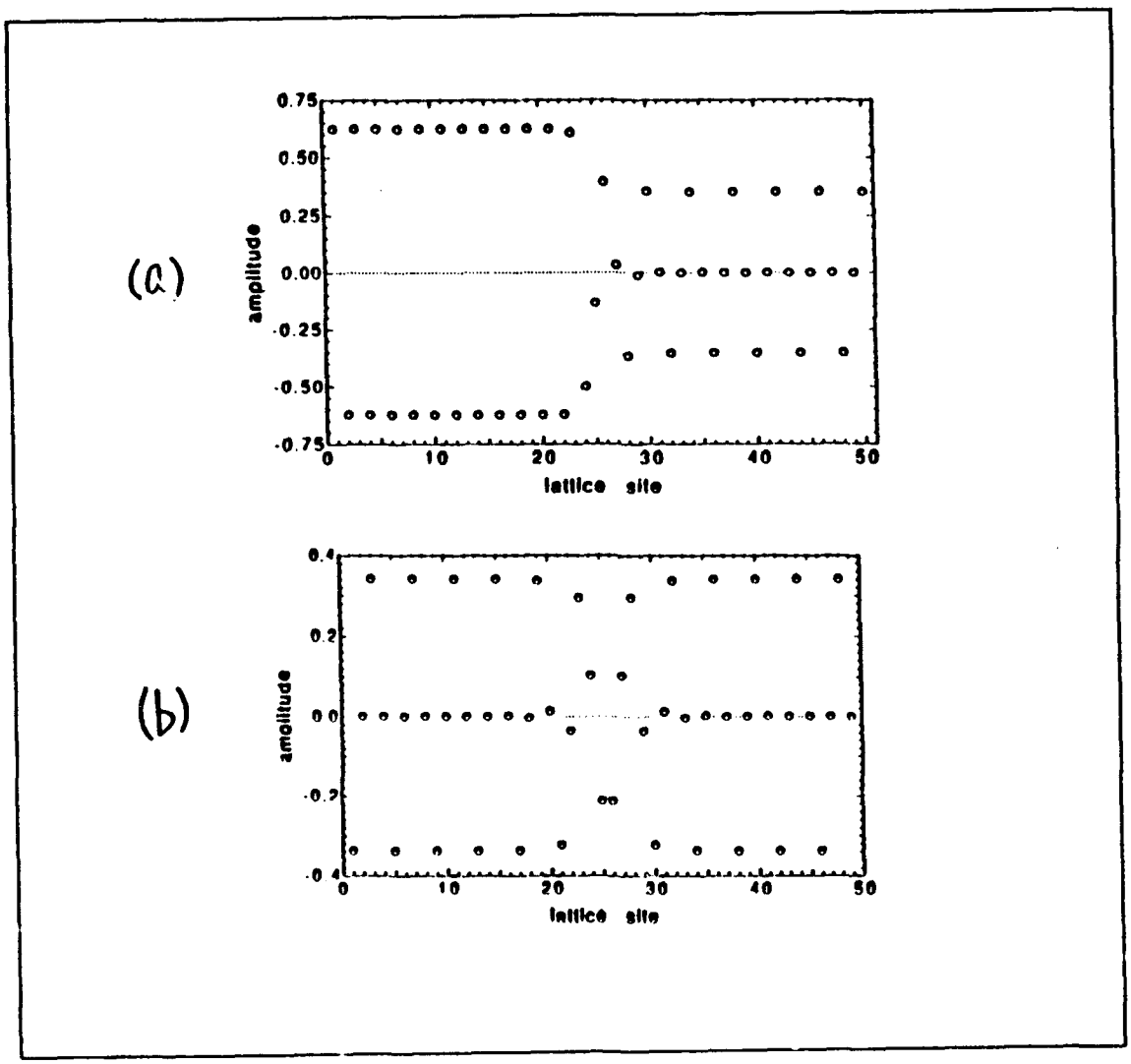

Fig. I.3. Localized structures in a nonlinear lattice of coupled oscillators: (a) domain wall between the upper cutoff mode (with a wavelength of two lattice spacings) and the wavelength-four mode, and (b) kink in a noncutoff (wavelength-four) mode.

II. THEORY

Many of the ideas about dispersive nonlinear waves originate in the problem of water waves. Our belief that kinks assists mode hopping and its connection to diode lasers is not an exception. In this chapter we turn explicitly to the problem of steady state kinks on standing surface waves. This will be done within the average variational approach (Whitham, 1965), from which we can obtain qualitative knowledge of the amplitude and wave number modulations. Quantitative knowledge demands that we relax both slowly varying and weakly nonlinear assumptions, which are implicitly assumed in the average Lagrangian technique (shown below).

A. DERIVATION OF THE MODULATION EQUATION

We consider the oscillatory part of the motion of an incompressible inviscid fluid in a homogeneous gravitational field. The depth of the fluid is infinite and the undisturbed fluid surface coincides with the xy plane at z=0, where z labels the vertical coordinates away from the surface. Potential flow is assumed and effects due to surface tension are neglected. The potential φ in the whole fluid satisfies Laplace's equation, as well as the condition $\partial\varphi/\partial z \to 0$ as $z \to -\infty$.

The variational principle (Luke, 1967)

$$\delta \int_R L \, d\bar{r} \, dt = 0, \tag{II.A.1}$$

$$L = -\rho \int_{-\infty}^{\zeta} \left\{ \varphi_t + \tfrac{1}{2}(\nabla\varphi)^2 + \tfrac{1}{2}\left(\frac{\partial\varphi}{\partial z}\right)^2 \right\} dz - \frac{\rho}{2} g\zeta^2, \tag{II.A.2}$$

gives Laplace's equation with the appropriate boundary conditions. Here R is an arbitrary region in the $(\bar{r}, t)$ space where $\bar{r}$ labels the coordinate of a point at the

surface of a liquid of density ρ, and ∇ is the two-dimensional gradient in the xy plane.

For a small change $\delta\varphi$ in φ,

$$
\begin{aligned}
-\delta\int_R \frac{L}{\rho}\,d\vec{x}\,dt &= \int_R\left\{\int_{-\infty}^{\zeta}\left(\delta\varphi_t + \nabla\varphi\nabla\delta\varphi + \frac{\partial\varphi}{\partial z}\frac{\partial\delta\varphi}{\partial z}\right)dz\right\}d\vec{r}\,dt \\
&= \int_R\left\{\frac{\partial}{\partial t}\int_{-\infty}^{\zeta}\delta\varphi\,dz + \nabla\cdot\int_{-\infty}^{\zeta}\nabla\varphi\delta\varphi\,dz\right\}d\vec{r}\,dt \\
&\quad -\int_R\left\{\int_{-\infty}^{\zeta}\left(\nabla^2\varphi + \frac{\partial^2\varphi}{\partial z^2}\right)\delta\varphi\right\}d\vec{r}\,dt \qquad \text{(II.A.3)} \\
&\quad -\int_R\left[(\zeta_t + \nabla\varphi\cdot\nabla\zeta - \varphi_z)\delta\varphi\right]_{z=\zeta}d\vec{r}\,dt \\
&\quad +\int_R(\varphi_z\delta\varphi)_{z=-\infty}d\vec{r}\,dt\ .
\end{aligned}
$$

the first term vanishes if $\delta\varphi$ is chosen to vanish on the boundaries of R. The stationary principle for (II.A.3) then implies:

$$
\begin{aligned}
&\nabla^2\varphi + \frac{\partial^2\varphi}{\partial z^2} = 0\ ,\quad -\infty < z < \zeta\ , \\
&\zeta_t + \nabla\varphi\cdot\nabla\zeta - \frac{\partial\varphi}{\partial z} = 0\ ,\quad z = \zeta, \qquad \text{(II.A.4)} \\
&\frac{\partial\varphi}{\partial z} = 0\ ,\quad z\to-\infty.
\end{aligned}
$$

For a variation $\delta\zeta$ in (II.A.1 & II.A.2)

$$
\delta\int_R L\,d\vec{r}\,dt = -\rho\int_R\left[\varphi_t + \tfrac{1}{2}(\nabla\varphi)^2 + g\zeta\right]_{z=\zeta}d\zeta\,d\vec{r}\,dt = 0\ ,
$$

it follows Bernoulli's law that at the free surface:

$$
\phi_t + \tfrac{1}{2}(\nabla\varphi)^2 + \tfrac{1}{2}\left(\frac{\partial\varphi}{\partial z}\right)^2 + g\zeta = 0\ ,\ z = \zeta\ . \qquad \text{(II.A.5)}
$$

Equations (II.A.4) and (II.A.5) are the equations for deep gravity waves in the surface of a liquid. They follow from the variational principle (II.A.1 & II.A.2).

We now study modulations of a one dimensional standing wave in the x direction for which

$$\varphi \approx \phi \cos\theta e^{i\omega t} + c.c. \ , \qquad \text{(II.A.6)}$$

where θ is defined such that

$$\theta_x = k \ , \qquad \text{(II.A.7)}$$

with wave number k and amplitude ϕ slowly varying functions of position x. In order to simplify the algebra we will consider up to quadratic terms in the amplitude in the Lagrangian density L and average over one period. This procedure eliminates the fast variation leaving only the corrections due to slow modulations of ϕ and k of an otherwise linear problem.

To proceed further, consider the solution to Laplace's equation

$$\varphi = \left\{ \phi \cos\theta + z\phi_x \sin\theta + \frac{z}{2k}\phi k_x \sin\theta \right\} e^{kz} \cos\omega t \qquad \text{(II.A.8)}$$

valid up to the leading orders in the derivatives of the slowly varying functions k and ϕ. Inserting the solution (II.A.8) into the Lagrangian density (II.A.2) and averaging over the fast variables θ and ωt we get

$$\mathcal{L} \equiv \frac{1}{\rho}\langle L \rangle = \tfrac{1}{4} a\phi\omega - \tfrac{1}{8} k\phi^2 - \tfrac{1}{16}\phi_x^2 - \frac{1}{64k^3}\phi^2 k_x^2 - \frac{\phi\phi_x k_x}{32k^2} - \tfrac{1}{8} g a^2 \qquad \text{(II.A.9)}$$

where we have set the surface height

$$\zeta = a\cos\theta \sin\omega t \, . \qquad \text{(II.A.10)}$$

A variation of the average Lagrangian (II.A.8) with respect to a yields the relation

$$a = \phi\frac{\omega}{g}, \qquad \text{(II.A.11)}$$

from which we obtain

$$\mathcal{L} = \tfrac{1}{8}\phi^2\left(\frac{\omega^2}{g} - k\right) - \frac{1}{16k}\phi_x^2 - \frac{1}{64k^3}\phi^2 k_x^2 - \frac{1}{32k^2}\phi\phi_x k_x \qquad \text{(II.A.12)}$$

A variation in θ and ϕ results in the expressions

$$\phi^2 = \text{constant}, \qquad \text{(II.A.13)}$$

$$\frac{\omega^2}{g} - k - \frac{3k_x^2}{8k^3} + \frac{k_{xx}}{8k^2} = 0 . \qquad \text{(II.A.14)}$$

Equation (II.A.12) corresponds to the constancy of the flux of wave action while Equation (II.A.13) represents modifications in the frequency due to amplitude modulations of the wave.

The crucial qualitative change of nonlinearity is the dependence of the frequency ω on the amplitude ϕ, which couples (II.A.12) and (II.A.13). For moderately small uniform amplitude ω may be expressed in Stokes fashion as

$$\omega^2 = gk - k^4\phi^2 \qquad \text{(II.A.15)}$$

corresponding to a frequency shift due to nonlinearities. The variational approach requires very little modifications to study modulations of nonlinear waves. The main questions to be addressed are the functional form to replace (II.A.6) or (II.A.8), and the details of the averaging. The major difference is that the average Lagrangian does not depend quadratically on the amplitude. Higher order amplitude terms modify the frequency of the uniform state according to (II.A.15).

The effects of nonlinearity in (II.A.15) can be added to the linear result (II.A.14) if the frequency shift due to amplitude modulations is of the same order

as the nonlinear frequency shift due to finite amplitude waves. Considering this situation to prevail we get from (II.A.13) to (II.A.15)

$$\omega^2 - gk + \phi^2 k^4 + \frac{g}{8k^2} k_{xx} + \frac{3}{2} \frac{d}{dk}\left(\frac{g}{8k^2}\right) k_x^2 = 0 \quad . \qquad \text{(II.A.16)}$$

Which describes the functional behavior of the k as a function of x for an amplitude and wave number modulated standing wave.

B. EQUIVALENT SINGLE OSCILLATOR APPROACH

Equation (II.A.15) can be further simplified by considering the hodographic transformation $v = k_x$. Thus,

$$k_{xx} = \frac{dk}{dx}\frac{dv}{dk} = \tfrac{1}{2}\frac{d}{dx}v^2 \quad . \tag{II.B.1}$$

If we define $a(k) = \omega^2 - gk + \phi^2 k^4$ and $b(k) = \frac{g}{8k^2}$, then Equation (II.A.15) becomes:

$$a + \tfrac{1}{2}b\frac{dv^2}{dk} + \tfrac{3}{2}\frac{db}{dk}v^2 = 0 \quad , \tag{II.B.2}$$

which can be integrated once to yield

$$v^2 = \frac{16}{g}k^3\left(\frac{\omega^2}{3} - \frac{gk}{2} - \phi^2 k^4 + k^3\alpha\right) \quad , \tag{II.B.3}$$

where α is a constant. We have thus reduced a second order differential equation to a first order equation. Equation (II.B.3) is equivalent to the equation of a particle of unit mass and zero energy in a potential well

$$U(k) = \frac{8}{g}k^3\left[\frac{gk}{2} + \phi^2 k^4 - \frac{\omega^2}{3} - k^3\alpha\right] \quad . \tag{II.B.4}$$

To evaluate the constant α in (II.B.4) we need to know the value of $k_x(U(k))$ as $x \to \infty$. For a localized structure this means that the value of k as $x \to \infty$ must be a constant k_0 for which k_x=0, that is

$$\alpha = \frac{1}{k_0^3}\left(\frac{gk_0}{3} + \phi^2 k_0^4 - \frac{\omega^3}{3}\right) \quad . \tag{II.B.5}$$

Note that this also corresponds to an extremum of (II.B.4).

Equation (II.B.3) is now properly posed for numerical integration, with the added advantage that it can be thought of as an initial value problem rather than a boundary value problem.

C. NUMERICAL ANALYSIS OF THE MODULATIONAL EQUATION

Using numerical methods the velocity equation (II.B.3) can be integrated and the wave profile determined. As a first step in this process we must define some dimensionless variables in order to facilitate computing:

$$X = k_0 x \qquad v = \frac{k_x}{k_0^2}$$

$$q = \frac{k}{k_0} \qquad \Phi^2 = \frac{\phi^2 k_0^3}{g}$$

$$\Omega^2 = \frac{\omega^2}{g k_0} = 1 - \frac{\phi^2 k_0^3}{g} = 1 - \Phi^2 \qquad \text{(II.C.1)}$$

using these definitions the right side of equation (II.B.3) can be rewritten in dimensionless form as:

$$v^2 = 16q^3\left[\frac{\Omega^2}{3} - \frac{q}{2} - \Phi^2 q^4 - q^3\left(\frac{\Omega^2}{3} - \frac{1}{2} - \Phi^2\right)\right]. \qquad \text{(II.C.2)}$$

In dimensionless form the potential well (II.B.4) is:

$$U(q) = 16q^3\left[-\tfrac{1}{3}\left(1-\Phi^2\right) + \tfrac{1}{2}q - \tfrac{1}{6}\left(1+8\Phi^2\right)q^3 + \Phi^2 q^4\right], \qquad \text{(II.C.3)}$$

and is plotted in Figure II.C.1. Note that at the value q=1 the potential energy is equal to zero; this follows from our assumption that the wave number in the wings is a constant. Moreover, as noted before the first derivative of the potential energy is also equal to zero at this point. Our goal in the numerical integration of Equation (II.C.3) can be described in terms of a graphical analogy. Imagine a marble placed at the intersection of the potential energy curve and the q axis to the right of q=1, we will call this point q_{max}. If this marble is released from rest at this point, because the system is conservative it will come to rest, after an infinite time, at the point q=1. We are interested in the form of the potential energy curve between these two points. If we can find q_{max}

analytically we can make our programming task easier by making an initial value problem out of boundary value problem. An initial value problem lends itself to numerical integration since we can take extremely small steps and trace out the curve using a simple iterative technique.

To make this simplification however, we must find q_{max}. From its definition q_{max} satisfies the equation U(q)=0 which implies:

$$-\tfrac{1}{3}\left(1-\Phi^2\right)+\tfrac{1}{2}q-\tfrac{1}{6}\left(1+8\Phi^2\right)q^3+\Phi^2q^4= \\ (q-1)^2\left(\alpha q^2+\beta q+\gamma\right)=0\,. \qquad \text{(II.C.4)}$$

Where we have used the fact that U has a double zero at q=1. Solving for the coefficients α, β, and γ we obtain

$$\alpha=\Phi^2$$
$$\beta=-\tfrac{1}{6}\left(1-4\Phi^2\right)$$
$$\gamma=-\tfrac{1}{3}\left(1-\Phi^2\right) \qquad \text{(II.C.5)}$$

For the solution, q_{max} must satisfy equation $\alpha q^2+\beta q+\gamma=0$ or,

$$q=\frac{1}{2\alpha}\left(-\beta+\sqrt{\beta^2-4\alpha\gamma}\right)\,. \qquad \text{(II.C.6)}$$

Since we used perturbation theory in the derivation of this equation we must observe $\Phi<1$. Hence, $\gamma<0$ and the desired root is then:

$$q_{max}=\frac{1}{12\Phi^2}\left[1-4\Phi^2+\sqrt{1+40\Phi^2-32\Phi^4}\right]\,. \qquad \text{(II.C.7)}$$

Using this equation to find our initial value we can use iterative techniques to plot the potential energy equation.

Equation (II.C.3) can be integrated by Euler-Cromer method. Because the marble will take an infinite amount of time to come to rest at the point q=1, our technique is numerically unstable. Since the computer cannot take infinitely

small steps it will inevitably under or over shoot the metastable point at q=1 and the marble will not come to rest. Figure II.C.2 is a plot of this integration for positive values of x. The values of the dimensionless constants were chosen to closely match those of our experimental system. Note that the dimensionless wave number increases as we approach the origin. The amount and rate of the change in q is determined primarily by the value of Φ. Note also that in order to decrease the numerical instability of this system five million time steps were taken to plot this graph.

The kink we are interested in incorporates both a modulation of wave number and amplitude. To determine the modulation of the wave surface as given by Equation (II.A.9) we need to determine the quantities a and θ. To determine the value of a we look at the adiabatic invariant (II.A.10) and express it in dimensionless terms:

$$A = \sqrt{\Phi^2 q} \quad , \qquad \text{(II.C.8)}$$

where A is the dimensionless amplitude. Implicit in (II.A.9) is the definition that $\theta_x \equiv k$ so we can find the value of θ using an iterative technique at the same time we are finding q. We will use the definition that for a small dx, $\theta = \theta + q dx$. We incorporated the values of ζ into our numerical integration algorithm and, for the same parameters used in the previous figure, produced Figure II.C.3. The amplitude does indeed increase with increasing wave number, but while the kink does posses the general characteristics of the observed wave it does not spread out over a large number of wavelengths. However, the theory does not take several possible important effects into account such as drive, dissipation, and surface tension. The failure to spread over many wavelengths prevents us from

effectively comparing these results to those found in the experiment in other than general terms. This is an area of continued effort.

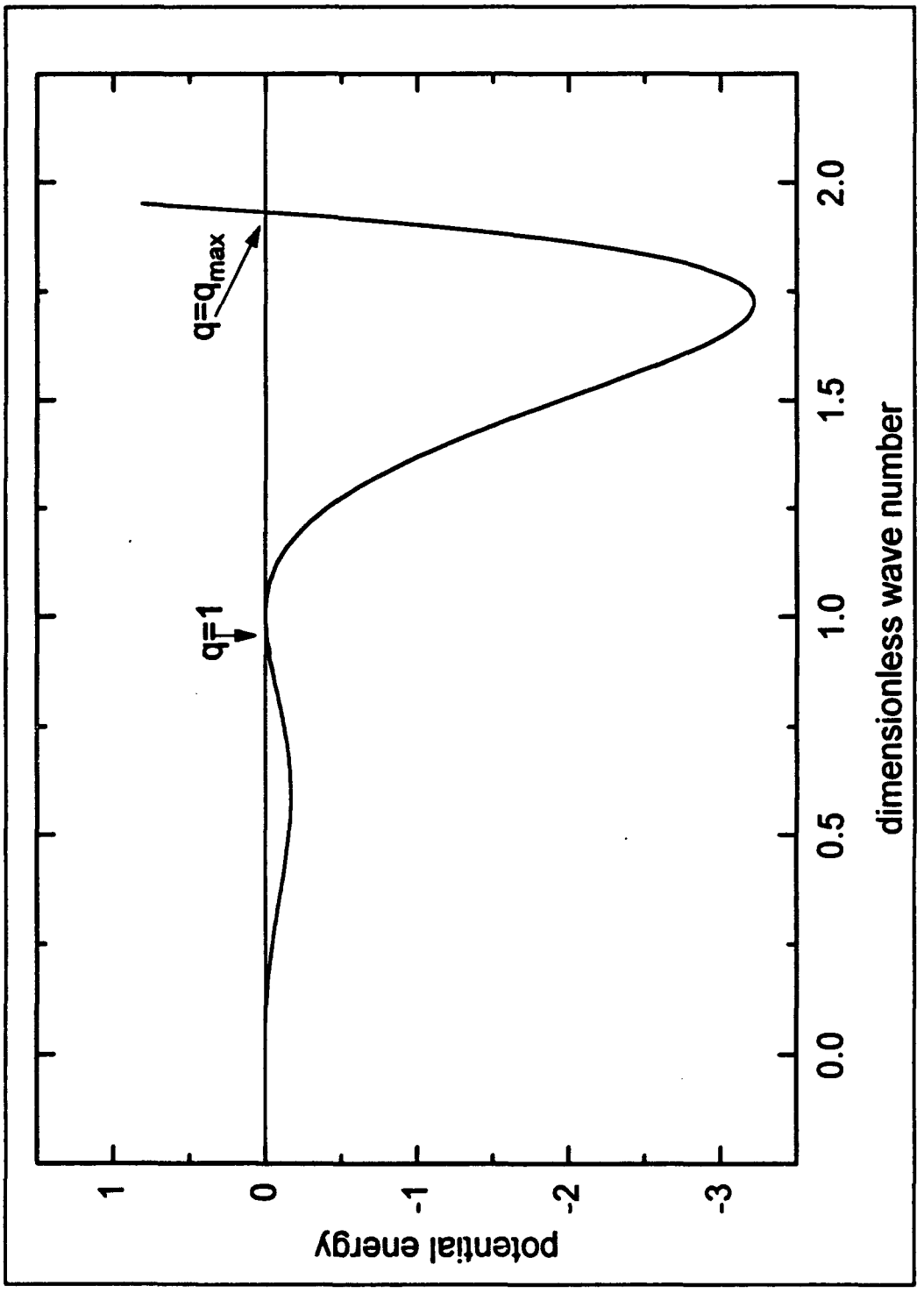

Figure II.C.1: Plot of the potential energy function for $\Phi = 0.35$

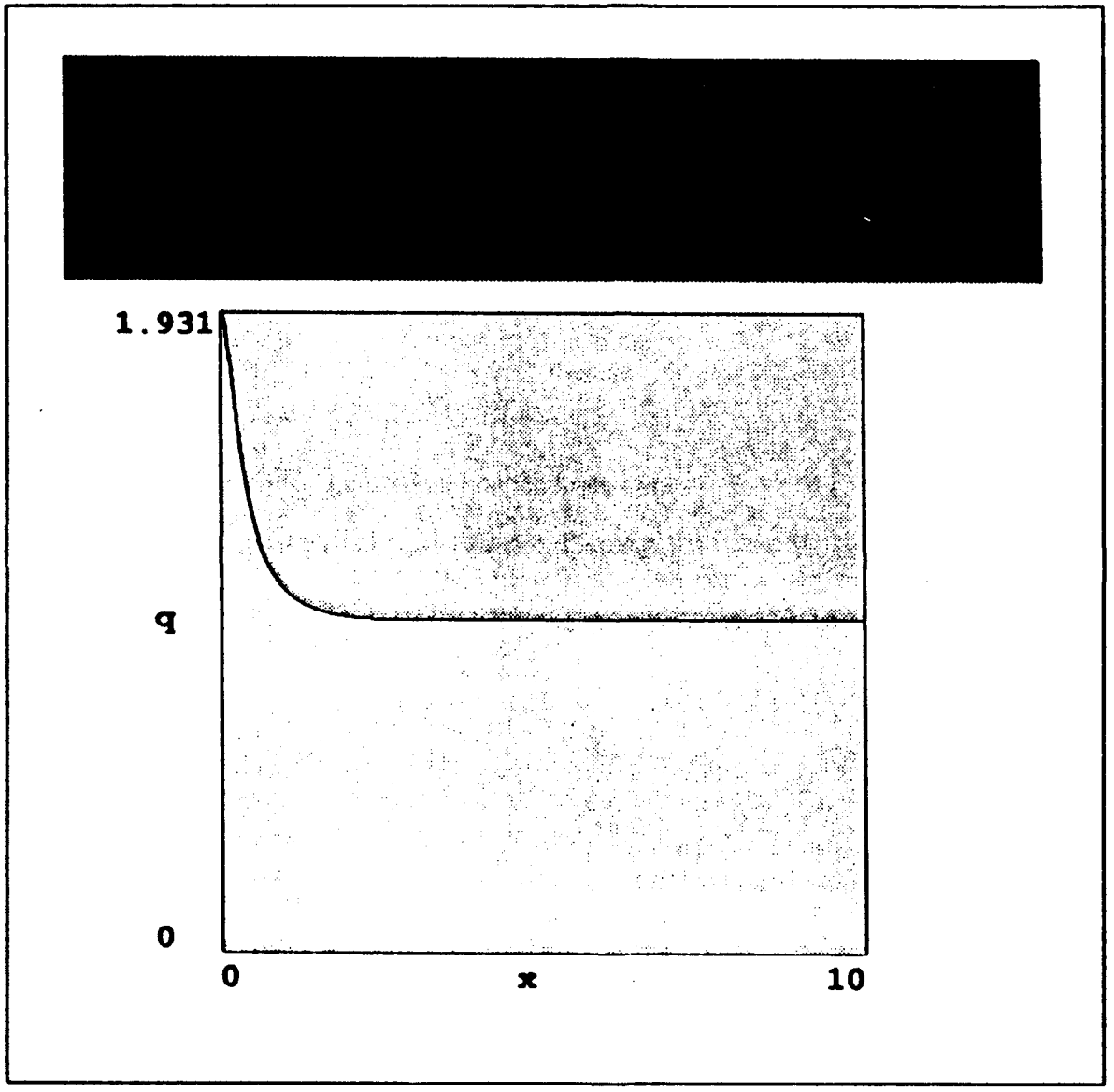

Figure II.C.2. P'ot of the variation of wave number with position from the origin.

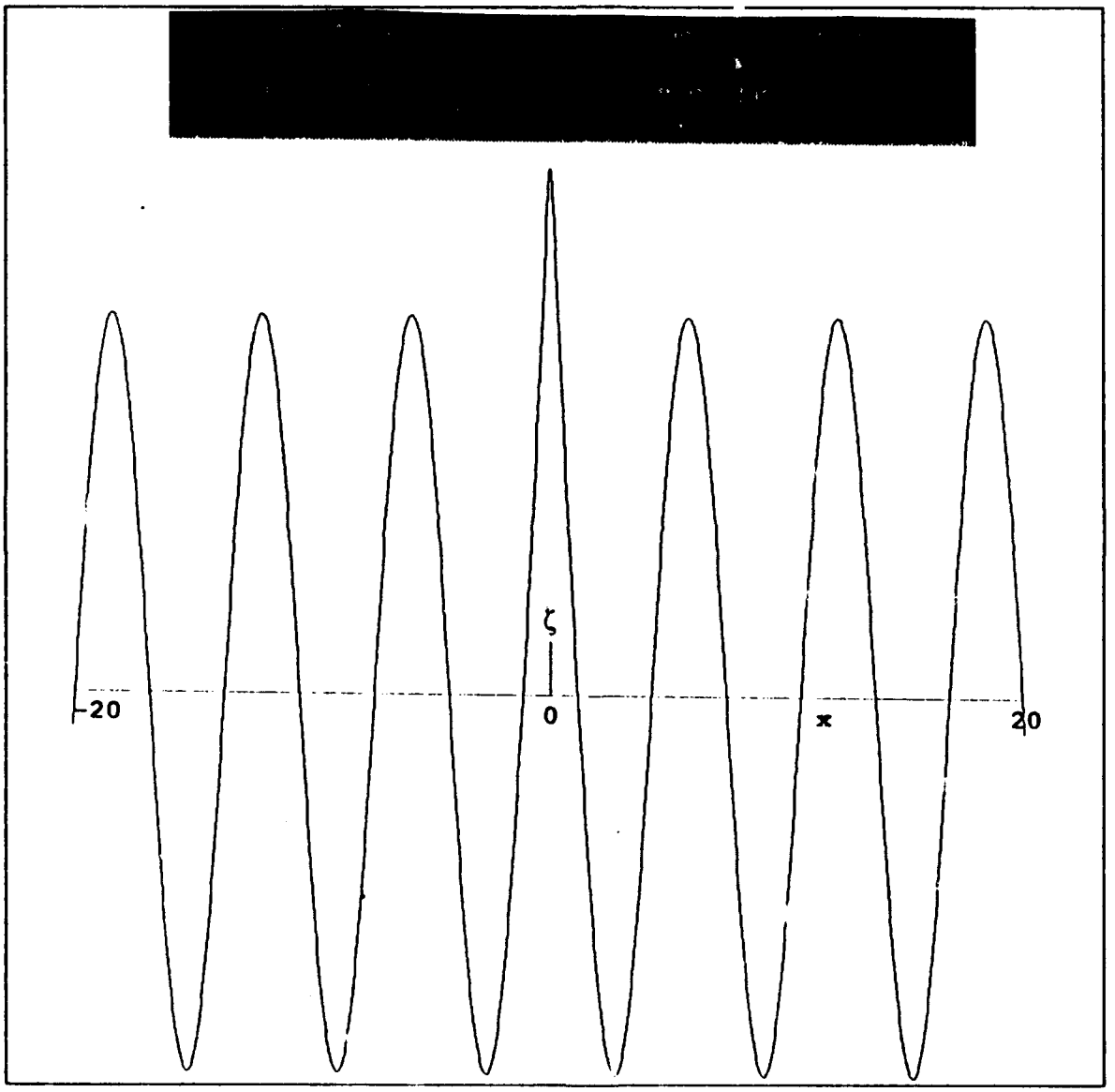

Figure II.C.3. Free surface profile as predicted by theory. Notice the kink, located at the origin, is a modulation of both wave number and amplitude.

D. THEORETICAL DRIVE PLANE

Figure II.D.1 shows the drive parameter plane regions in which the sixth and seventh modes exist. The curves are based on treating each mode as a single oscillator, where the amplitude is at most a function of time. The surface height as a function of position x and time t is then

$$\zeta(x,t) = A(t)\cos(kx)e^{i\omega t} + c.c. + \cdots, \qquad \text{(II.D.1)}$$

where the amplitude A is in general complex, k is the wave number, ω is the frequency, and the ellipsis denotes higher harmonics in space and time. In the fundamental equations of motion for surface gravity waves on a deep liquid, we include parametric drive by replacing the acceleration g due to gravity by $g + 4d\omega^2\cos(2\omega t)$, where d is the displacement amplitude of the drive and 2ω is the drive frequency. Linear damping is included phenomenologically such that the free response amplitude decays as $A(0)e^{\frac{-\beta t}{2}}$. By substituting (II.D.1) in these equations, and assuming that the wave is weakly nonlinear and slowly varying in time, and that the drive and dissipation are weak, we obtain the evolution equation

$$2i\omega\, dA/dt + \left(\omega_o^2 - \omega^2 + i\omega\beta\right)A + 2\omega^2 k d A^* = \Gamma\omega^2 k^2 |A|^2 A, \qquad \text{(II.D.2)}$$

where $\omega_o = (gk)^{1/2}$ is the linear frequency of the mode, and Γ is the dimensionless nonlinear coefficient which is +1 in our case. Two instabilities are implied by (II.D.2). The first is obtained from the stable steady-state solution, which is given by $A = Ae^{i\delta}$, where

$$A = \frac{1}{\omega k \Gamma^{\frac{1}{2}}} \left[\omega_o^2 - \omega^2 + 2\omega \left(k^2 d^2 - \beta^2 / 4\omega^2 \right)^{1/2} \right]^{1/2}, \qquad \text{(II.D.3)}$$

and $\tan(2\delta) = \beta(\omega^2 k^2 d^2 - \beta^2)^{-1/2}$. For $\omega > \omega_o$, (II.D.3) implies that the minimum drive amplitude to maintain the response is

$$d = \frac{1}{2\omega^2 k} \left[\left(\omega_o^2 - \omega^2 \right)^2 + \omega^2 \beta^2 \right]^{1/2}. \qquad \text{(II.D.4)}$$

The response amplitude approaches zero as this boundary is approached from above. For $\omega \leq \omega_o$, the minimum drive amplitude is given by the vanishing of the inner radical in (II.D.3), or $d = \beta/2\omega k$. Along this boundary, the response amplitude falls to zero from finite amplitude. This corresponds to the common point of the stable and unstable branches of the parametric steady-state response curve. This "closure" point arises because the acceleration amplitude of the drive decreases as the frequency is decreased and the displacement is held constant. The combined maintenance curves, for $\omega \leq \omega_o$ and $\omega \geq \omega_o$, are shown by solid curves in Figure II.D.1.

The second instability implied by (II.D.2) corresponds to excitation from rest, in which the nonlinear term is negligible. This yields a drive amplitude threshold that is identical to (II.D.4) but which now applies for $\omega \leq \omega_o$ as well as $\omega \geq \omega_o$. This is the well known Mathieu curve in the limit of weak drive, and is represented by dashed curves in Fig. II.D.1.

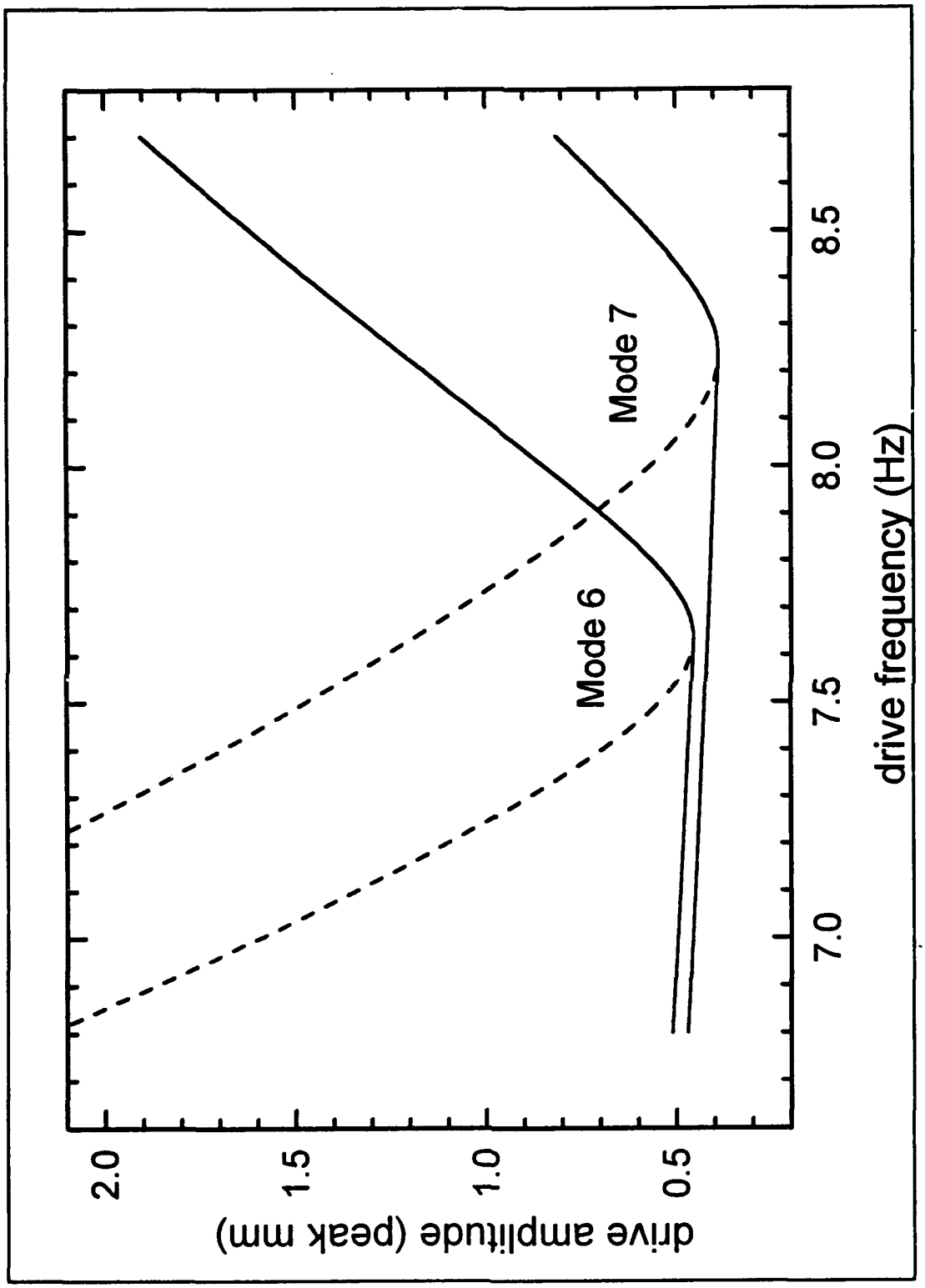

Firgure II.D.1. Plot of the theoretical drive plane.

III. EXPERIMENT

This chapter details the experimental apparatus and equipment, and the results. The experiment evolved from searching for a steady-state kink (described in Ch. II) to exploring the kink's role in mode hopping. We developed a qualitative description of the mode hopping process from the data, and also compared the data to theoretical predictions.

A. APPARATUS

The evolution of the experiment dictated the designs of the troughs. Initial uncertainty as to the number of wavelengths over which the modulations would occur led to a long straight trough. In this trough we observed the first occurrence of a kink and established a connection to mode hopping. However, we suspected that end-effects were preventing the existence of a steady-state kink. The second design featured an annular design to eliminate end effects, making the presence of a kink during mode hopping clearly visible. Both troughs contributed to the success of the experiment, though the quantitative experimental results are for the annular trough.

The straight trough design called for a one dimensional system with a length adequate for twenty wavelengths. This requirement arose because we did not know over how many wavelengths the kink would extend. We drove the trough parametrically at the center and adopted a rectangular design that would not allow flexing. The trough (Fig. III.A.I) was constructed from 3/8" polycarbonate sheet with a series of precision milled spacers. With the spacers temporarily in place, we affixed the walls of the trough to the base using Weldon. The trough has inner length of 1.000 m and an inner width of 1.5 cm. This length allowed for many wavelengths over which the kink could exist but it also

made it difficult to tell when a transition to an adjacent mode occurred. Even with beaches inserted, the ends of the trough attracted kinks and precluded observation of their profile. In addition, we determined that shaking the trough at the middle was unstable because an imbalance in the placement of the trough would cause a shift of water that would increase the imbalance. To eliminate this we drove the trough with two shakers but end effects and the small separation between modes prompted the second design.

We constructed the annular trough (Fig. III.A.2) in the hope of finding a steady-state kink. Using a lathe, we machined a step into the acrylic base a centimeter in width and a millimeter in height. This step provided a guide for the placement of the inner and outer walls. The walls were sections of acrylic tubing attached to the base with Weldon. We constructed a lid to allow the mounting and placement of a two wire probe. The base and lid had separate attachments to the shaker table so that we could rotate the top relative to the base while in use.

The choice of a liquid for the troughs proved equally important as the design of the troughs themselves. As will be discussed below, the kinks as first observed were violent. In the first trough we used water and a wetting agent Fotoflow with food coloring for visibility. The Fotoflow decreases the surface tension of the water much as does common soap. Unfortunately, it also created bubbles when agitated just as soap does. Worse, the bubbles would serve as nucleation sites for kinks and hampered transduction. For this reason, alcohol became the liquid of choice in both troughs with the coloring agent Fluorescein. This choice was not without its drawbacks however, as the alcohol attacks the

acrylic and forms stress cracks. The low viscosity and absence of bubbles made it an acceptable choice for this study.

The driver chosen for the troughs was the American Power Systems Model 114 shaker and amplifier (Fig. III.A.3). A HP 3325B synthesizer drove the amplifier. We monitored the amplifier output using a digital multimeter connected to the current sensor of the amplifier. The current sensor output provided 250 mV/Amp of drive and a maximum of 1 V. This combination provided a steady displacement suitable for all but the most extreme drive levels. A concrete table and leveler supported the trough. The leveler was constructed from a 1.5" thick and one foot square acrylic sheet. Three holes for 1/2"-32 bolts were drilled and the heads of the bolts were machined on a lathe so they contacted the table at a point which prevented them from "walking" when turned. Using a circular bubble level as a guide we could level the trough by turning the appropriate bolt.

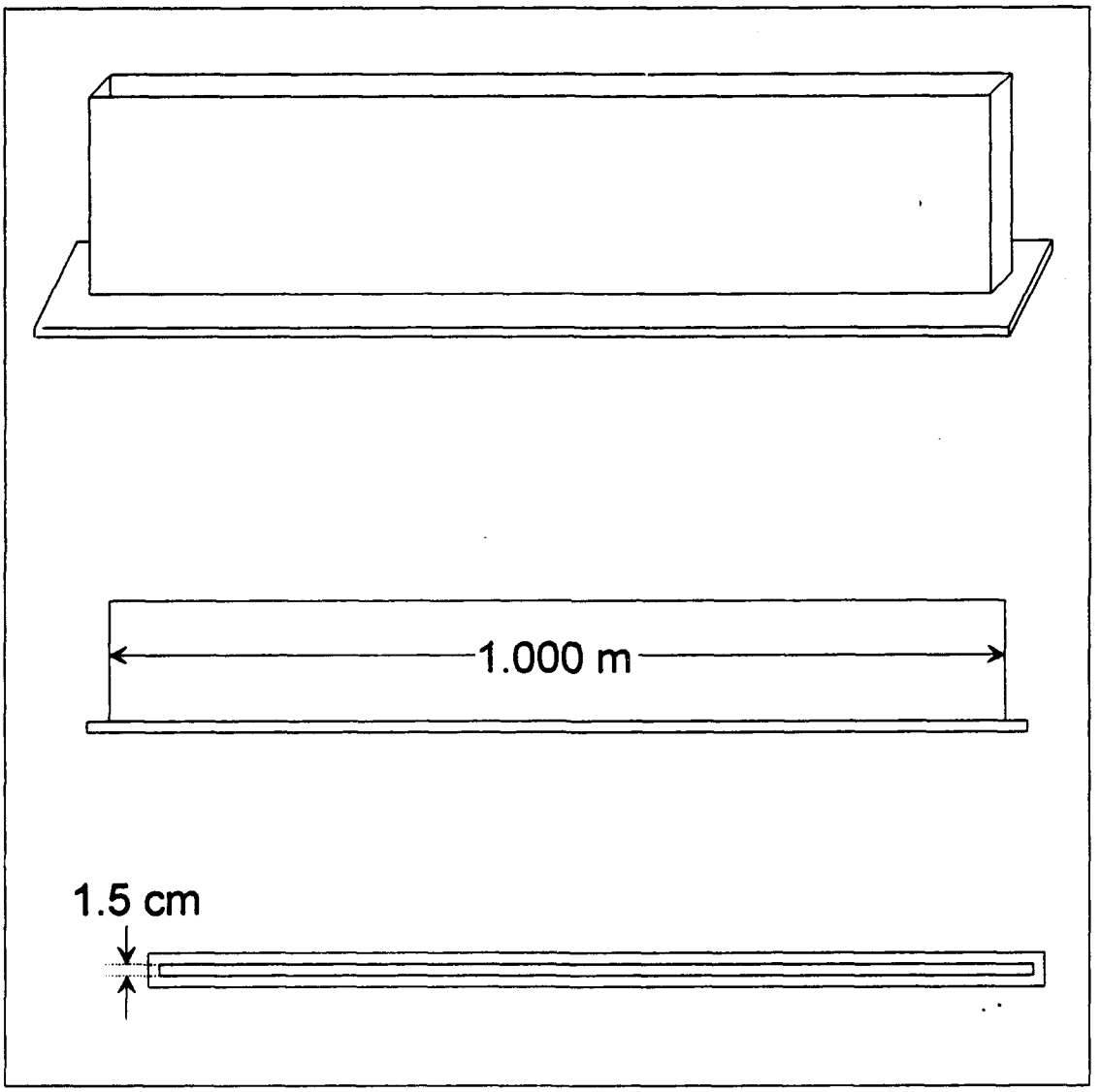

Figure III.A.1. The straight trough.

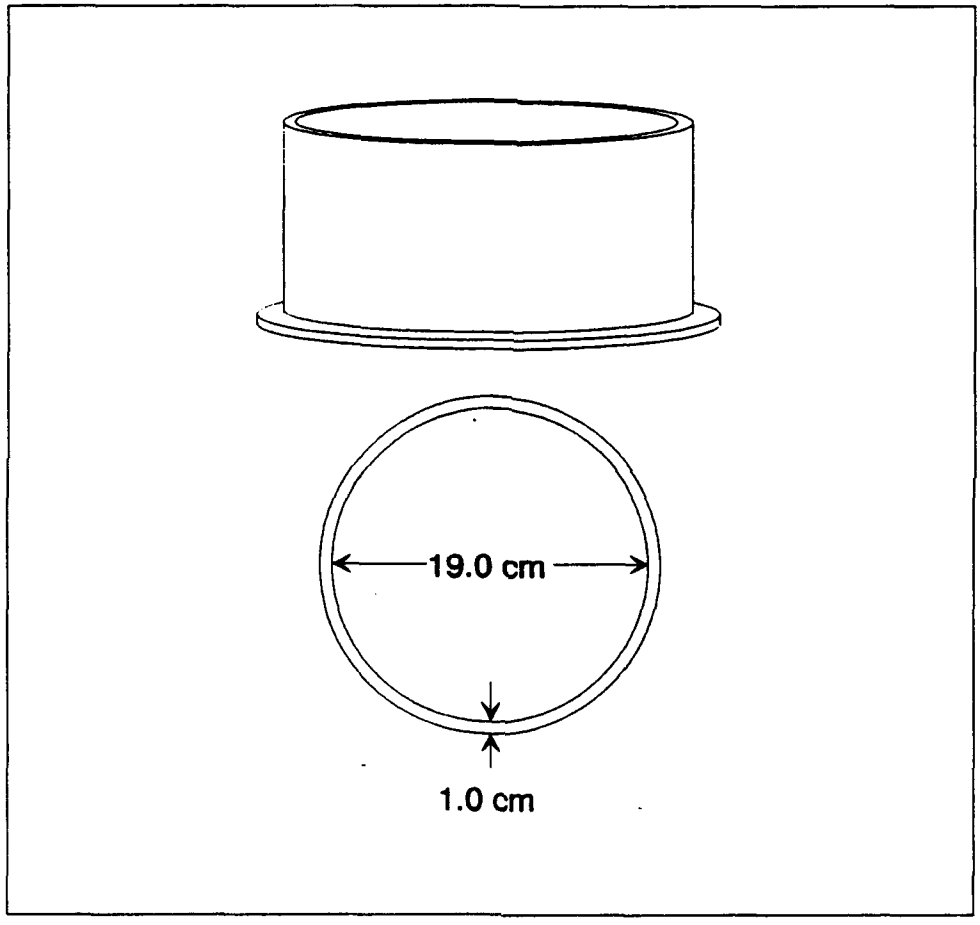

Figure III.A.2. Annular Trough design.

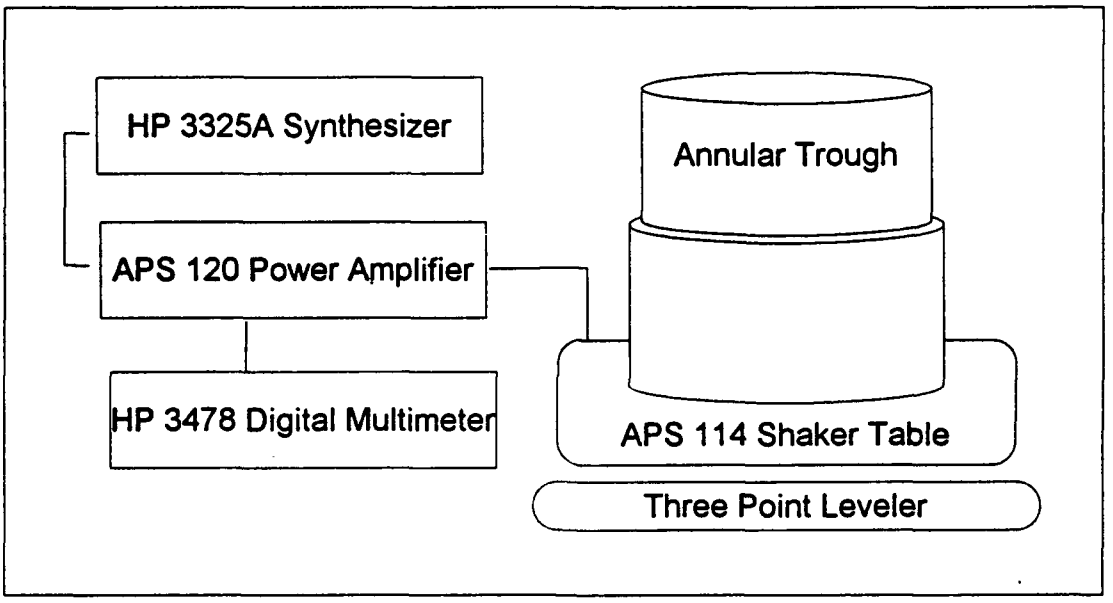

Figure III.A.3. Schematic showing the driver and its support equipment.

B. TRANSDUCTION

The measurement of the drive and steady-state response amplitudes was essential for comparison to theory. We also required surface height "snapshots" (at definite times) during the mode hopping transitions.

To determine the drive parameters we needed an accurate measure of both frequency and amplitude. The synthesizer provided a very precise measure of the drive frequency. To measure the amplitude of the shaker table, we employed a Linear Variable Differential Transformer (LVDT) (model number 30055112 Rev. L made by G. L. Collins Corporation) that gives a linearly varying signal over a large range of displacements. The LVDT consists of two primary and a secondary concentric solenoid. (The labels "primary" and "secondary" are arbitrary here). The two primary solenoids have opposite helicity and are connected in series. Within their core a permeable plunger moves with the object to be measured. The AC source drives the LVDT's primary solenoids and the secondary solenoid provides the output signal. If the plunger fills equal amounts of each of the primary solenoid's cavities the output will be zero; any movement of the plunger away from this zero point will create a non-zero response. This response will be linear if the displacement is less than a half-inch from the zero point. Outside this range end effects are no longer negligible.

We calibrated the LVDT statically. The value of this calibration factor depends on the drive applied to the primary solenoids and the demodulation of the signal. The output of the secondary solenoid is a modulated reference signal where the modulation amplitude is proportional to the displacement of the plunger. This signal is exactly equivalent to an AM radio signal, and is demodulated with a lock-in amplifier. A low pass filter then extracts the DC

signal. The static calibration factor is the change in LVDT output voltage per unit displacement of the plunger. For this calibration, we placed the LVDT in a calibration stand and measured displacement of the plunger with a micrometer. We obtained twenty data points over an inch range, and the slope of the line on which the points lay defined the calibration factor. The results of the calibration given in Figure III.B.1 show the high degree to which the response is linear.

To expedite the gathering of surface wave data, we conducted a second, dynamic, calibration that related the output of the LVDT to the synthesizer output. This dynamic calibration also had a dependence on the reference and lock-in amplifier settings but the two calibration factors could, in principle, combine to form a single calibration factor that would relate synthesizer voltage to displacement and be independent of the other aspects of the system. For this factor to be independent two conditions must be met: first, the amplitude of the shaker table must be independent of the mode in the trough -- a fact verified by experiment; second, the amplitude response of the shaker must be linear and the proportionality constant must be the same over the operating range of frequencies. To measure this we drove the trough at amplitudes that covered the entire operating range at a central frequency. We measured the component of the lock-in amplifier's signal at that frequency with a dynamic signal analyzer. Figure III.B.2 shows a deviation from linearity of up to ten percent. Thus a single calibration factor, independent of the settings of the reference signal and lock-in amplifier, is only a rough estimate; we found this number to be 1.38 mm/ Synthesizer V. The experimental data presented in the experimental results section have a nonlinear correction factor to compensate for this deviation.

Because we could not eliminate the lock-in amplifier settings from the calibration, they require some examination. The lock-in provided the reference signal of 5 kHz and 1 V to the LVDT; this frequency was chosen such that it was much greater than the drive frequency. We employed the EG&G model 5210 Lock-In Amplifier but the general components discussed are applicable to any lock-in amplifier. For our purposes, the lock-in amplifier's controls fall into five functional groups: signal input, pre-amplifier, phase control, DC offset, and post-amplifier. We set input sensitivity to 30 mV, the most sensitive possible. The pre-amplifier allows for the filtering of the input signal but any such filtering diminishes the signal available and thus none was used. Phase control can set the relative phase of the input and reference signals; the auto-phase function finds the point at which the in-phase component is a maximum. This phase is not exactly zero as the wiring of the LVDT has a finite impedance but it was at most a few degrees. The DC offset zeroed the signal if the LVDT was not operated about its zero-point. The post-amplifier provides both amplification and filtering to the output signal. Again because any filtering would diminish our signal and the dynamic signal analyzer could eliminate all unwanted components, this option was set to the minimum time-constant and roll-off. By recording the settings of the lock-in the values of the dynamic and static calibrations we reproduced measurements accurately.

We measured steady-state response amplitudes using a two-wire probe. This technique uses a small probe constructed of two parallel wires placed in the liquid. The resistance between the two-wires will vary proportionally with the height of the liquid as long as the liquid level does not approach the ends. We constructed a simple voltage divider circuit where the voltage of the output was

proportional to the liquid height. The output of a voltage divider circuit is given by:

$$V_{out} = \frac{V_{in} R_0}{R_{probe} + R_0} , \qquad \text{(III.B.1)}$$

where R_0 is the output resistor and R_{probe} is the resistance of the probe. The output will be proportional to the liquid height if the resistance of the probe is much larger than that of the output resistor. Then we can drop R_0 from the denominator in (III.B.1) and the two voltages will be proportional. In choosing an appropriate value of R_0 we found the largest value that would give a one part in one thousand error. We measured the mean resistance of the alcohol to be 10 MΩ and chose an output resistance of 10 kΩ. The two-wire probe was driven by another EG&G Model 5210 lock-in amplifier and its signal, identical in form to the output of the LVDT, was demodulated by the same lock-in amplifier.

Video techniques provided images of the kink in transition. We chose video data since it is non-intrusive and it provides the spatial density of samples needed for imaging a continuum. The video equipment used was a Sony 3CCD DXC-3000A camera and Sony U-Matic VCR model number VO-5800. We selected this system over one based on VHS or Super-VHS formats because they give only 30 frames a second of interlaced signal. The U-Matic system we chose produces 60 frames a second of non-interlaced images in an NTSC format acceptable to our frame grabber. This higher frame rate meant that with the approximately 16 frames taken during each period of the response we could forgo the tedious process of interpolating the amplitudes at the turning points. Because the wave spends a longer time at the turning points we calculated that our images yield amplitudes within two percent of the true values. We analyzed

the data taken in the lab using the slow motion and frame advance capabilities of the VCR. For the figures presented in this thesis and wave snapshots, we used "frame grabbing" techniques. Frame grabbing is the process in which video data is converted into digital computer data. We used a Macintosh II with the Perspectives Pixel Pipeline frame grabber board and Image v1.32 (Freeware from the NIH) for control. We used Image to acquire the data, encode it in a TIFF format file, and record the pixel coordinates of the liquid surface.

The most challenging aspect of transduction was the imaging of the entire trough through a transition. Because the trough was annular we could not film through the walls of the trough without a substantial portion being obscured. To allow the simultaneous imaging of the entire trough we used a conical mirror (Fig. III.B.3). This mirror was constructed from a single piece of acrylic turned to a cone on a lathe. The surface was polished to a high buff and coated with aluminum in a vacuum evaporator. This mirror fit inside the annular trough and from above provided a 360 degree perspective. The sides of the cone were oriented at 45 degree angles to the vertical such that vertical displacement of the liquid equaled the radial displacement of the image. The Angular resolution however, varied with displacement since the circumference of the cone was a function of height. This had the effect of "sharpening" the crests and "softening" the troughs of the projected image. To remove this effect and present the images in a form more readily understood we applied non-linear corrections to the images to make them appear they were taken from a rectangular trough. In the first step in this process we transferred the video images of the transition to digital computer images using a frame-grabber and extracted data points along the free surface from this digital data. These data points consisted of the pixel

coordinates of approximately three hundred samples to the free surface. The pixel coordinates were converted to a polar coordinate system. These data points were then "unwrapped" from the conical projection to a rectangular projection using an algorithm we developed using MathCad. A sample MathCad worksheet is provided in Appendix A.

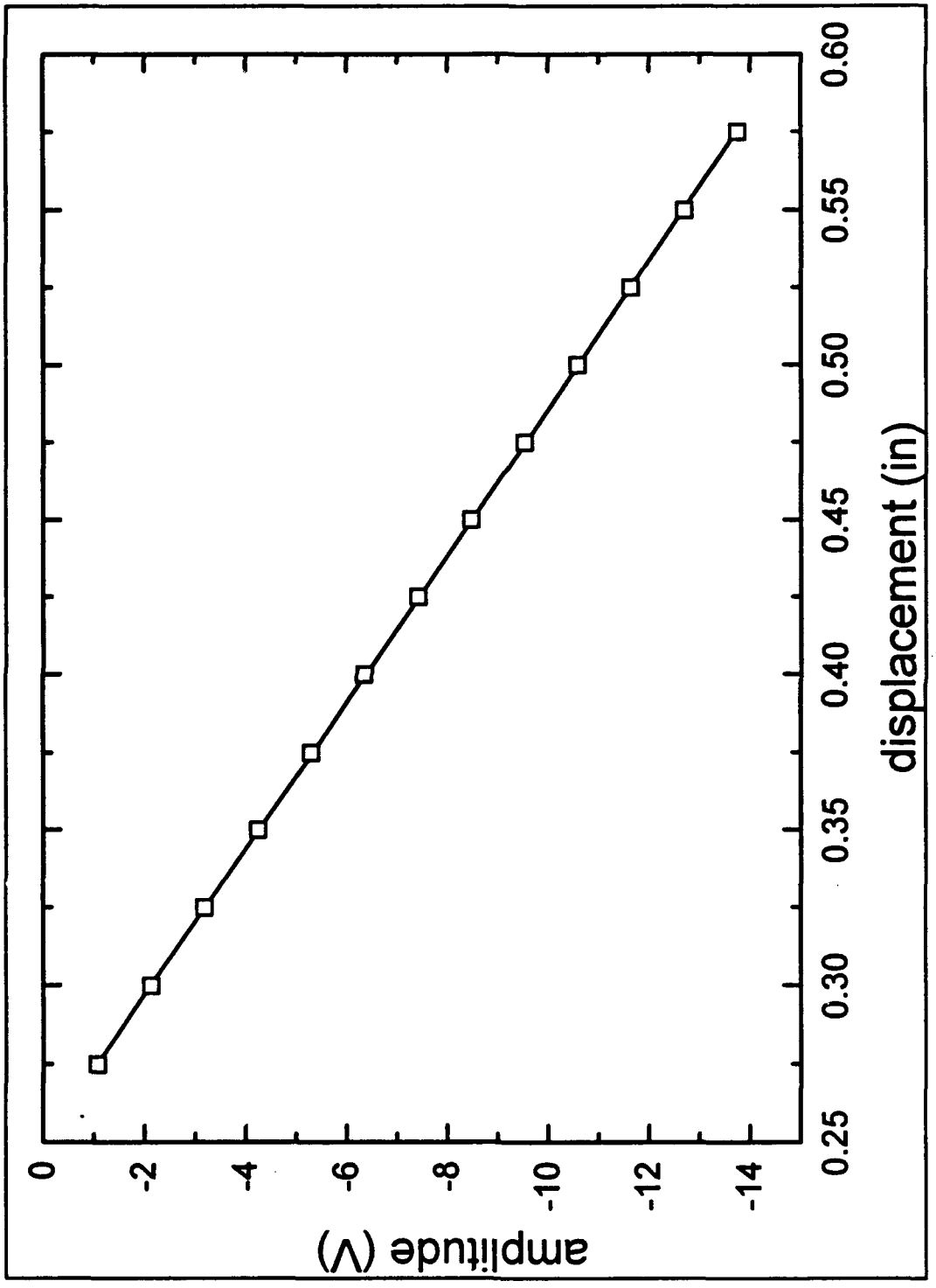

Figure III.B.1. Plot showing the static callibration of the LVDT results.

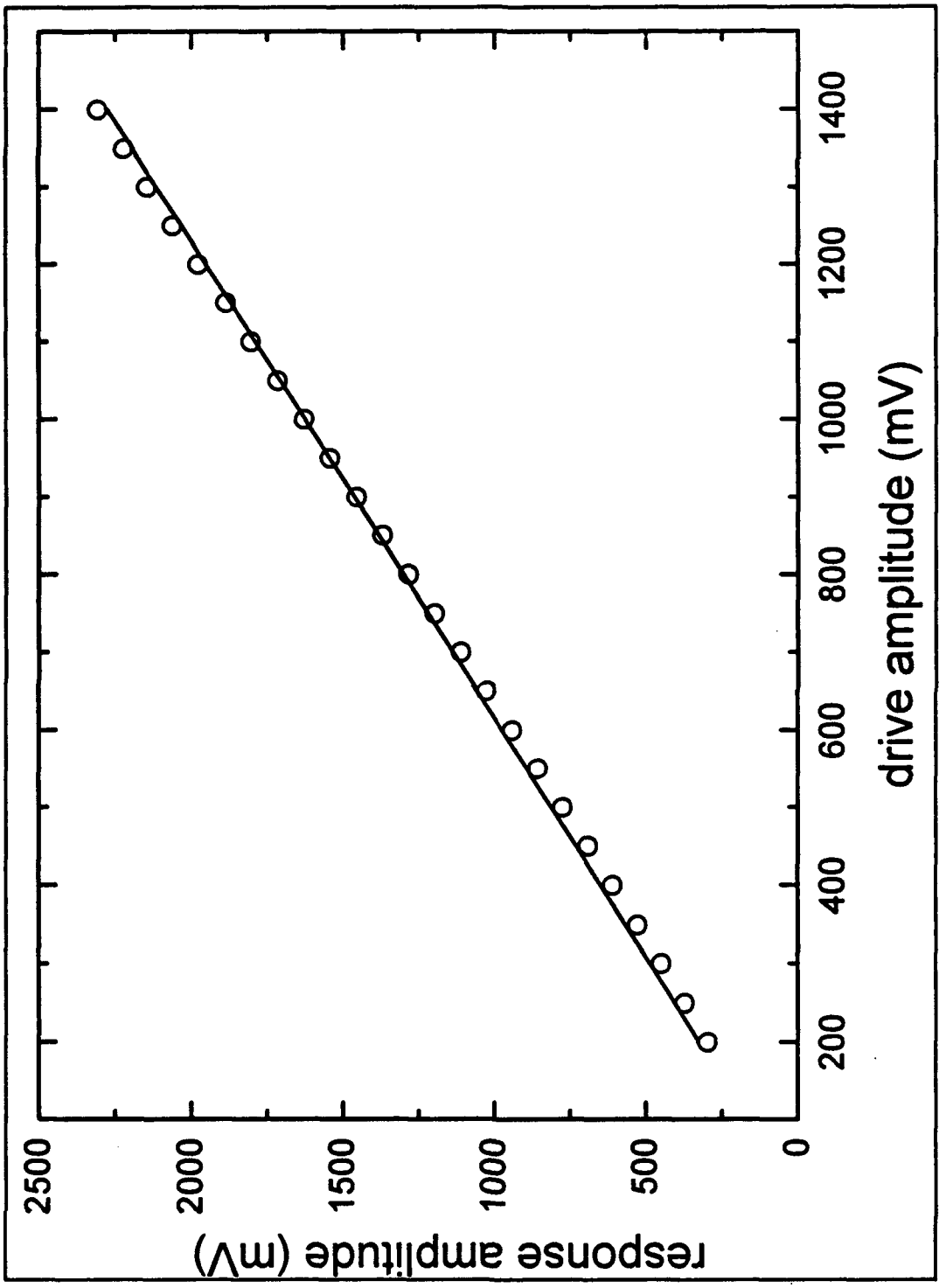

Figure III.B.2. Plot of the dynamic callibration of the LVDT.

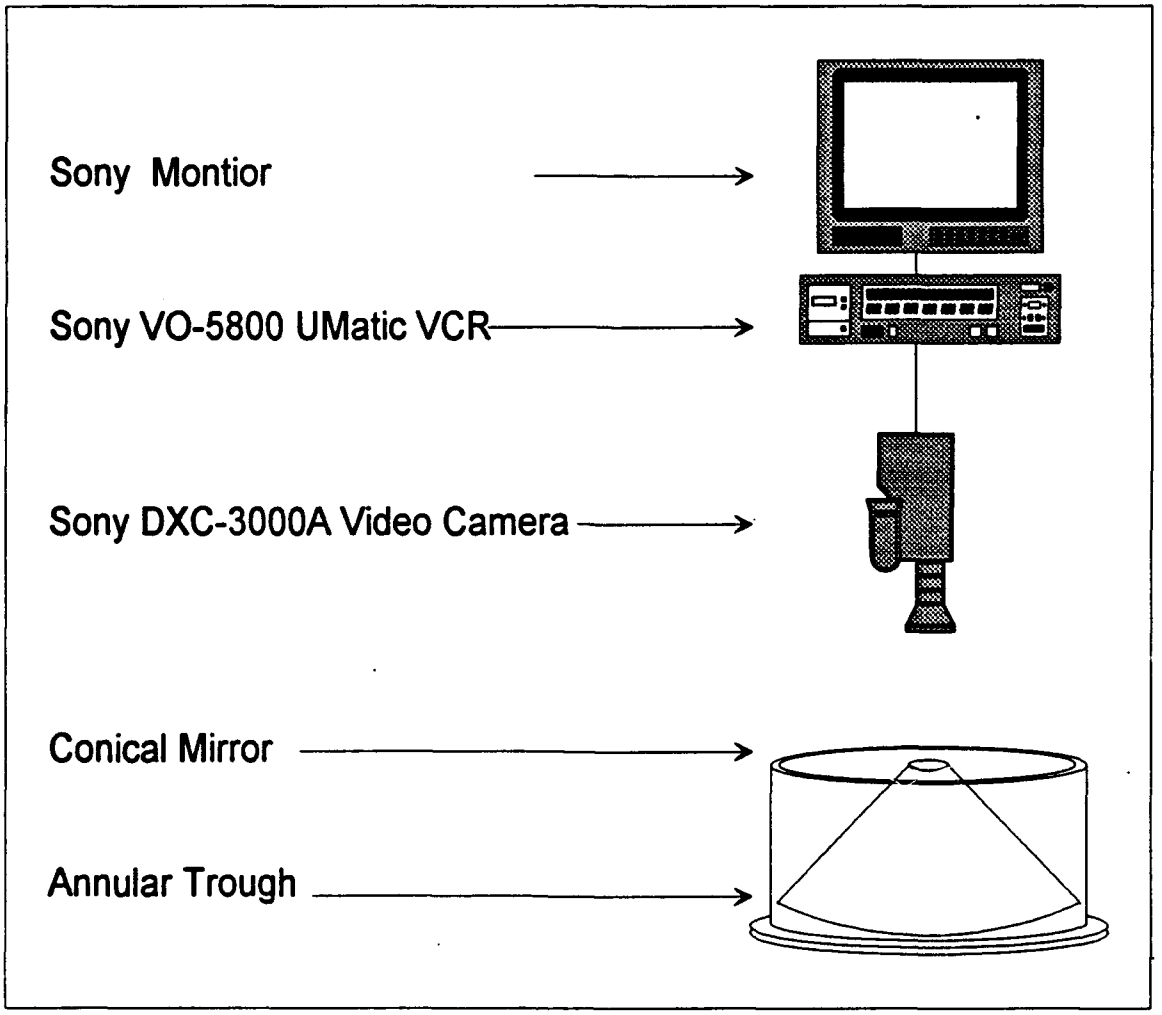

Figure III.B.3. Apparatus for th video transduction of the wave profile.

C. DRIVE PLANE

The results of the experiments carried out can be classified as follows. First, there is drive plane data which includes Mathieu Curves and kink-assisted mode hopping boundaries. Second, the hysteresis data provides another perspective on the mode hopping data. Finally, there is the actual images of the wave profiles in transition and an interpretation of the mechanisms of mode hopping.

We concentrated on two particular modes in out study of this system. Since the annular trough is constrained to periodic boundary conditions there can exist only an integer number of wavelengths for any steady-state mode. We chose the mode which contained six and seven wavelengths for study for the following reasons. At higher modes it was harder to distinguish between adjacent modes and eventually the wavelengths would become short enough that the transverse modes would be excited. Because this is a softening system lower modes required larger drive amplitudes which would have exceeded the capabilities of our driver. Once the modes were selected, we sought to find the drive parameters in which these modes existed. These areas were delineated by excitation from rest and maintenance curves. The excitation from rest curves represented the lowest possible drive levels at which a given mode would be excited at a given frequency. The growth rate of the curves at this drive level is infinitesimal so each data point would take an infinite amount of time to collect. Pinning and friction would not allow the theoretical values to be attained and thus an arbitrary time limit was set for a mode to be excited. The maintenance curves also represented minimum drive levels but these were the levels required

to maintain an existing mode at a given frequency. These curves were developed theoretically in Section II.D.

In order to present the theoretical curves and experimental points on the same plot we needed to input representative values for the needed constants. Three quantities were required: the dissipation parameter β; the wave number k_0, and the resonant frequency ω_0. The dissipation parameter was determined using the two-wire probe to measure amplitude as a function of time for a free decay. A straight line was then fit to the log of the amplitudes and β was taken to be twice the slope the line (Fig. III.C.1). The values of β found using this method were 1.61 s^{-1} for mode seven and 1.51 s^{-1} for mode six. The wave number was based on a wavelength found by dividing the mean circumference of the trough by the number of the mode. The wave numbers used were 61.96 m^{-1} for mode six and 72.31 m^{-1} for mode seven. The resonant frequency was found using the dispersion relation $\omega_0 = \sqrt{gk_0}$. The values found were 24.09 rad/sec for mode six and 26.03 rad/sec for mode seven. Using these values we could plot the theoretical curves with the experimental data points and expect fair agreement.

To create a consistent and accurate plot of the experimental drive plane we employed a series of rules. These rules set time limits for certain actions to occur and defined the procedures in which we handled and recorded the results. For the excitation from rest data the rules were as follows: first, we let the trough stand at rest for 30 seconds if a mode had not been excited and one minute if one had; second, we drove trough for two minutes or less at a drive level; third, if we observed the appearance of the mode we would stop the trough, record the drive level, increment the frequency 0.1 Hz, and begin again; if the time expired

without the mode appearing we would stop the trough and increment the drive level 10 mV. We obtained the maintenance data using similar rules except the mode died out instead of appeared and we recorded previous drive level. This data is shown in Figure III.C.2.

Evaluation of this data requires a reexamination of the theoretical drive plane. As discussed in Section II.D at the resonant frequency the maintenance and excitation from rest curves are coincident. This implies that the two data sets should be equal at the resonant frequencies. Instead, the excitation from rest curves are much higher than the corresponding maintenance curves. To explain this discrepancy we offer the following suggestions: first, at the true excitation from rest drive amplitudes the growth rate of the mode is infinitely small and may not be apparent after the two minute period; second, frictional effects such as scrubbing on the walls could damp out small amplitude motion; finally, the theory does not take the surface tension of the alcohol into effect. These effects, though present in both sets of data, can be imagined to have a lesser effect on a system with a mode already established. Because of this discrepancy the maintenance data alone appears in subsequent figures.

Figure III.C.3 shows, for mode seven, the disparity between the theoretical curve and the experimental points. To ensure correspondence we fit the theoretical Mathieu curves to the low amplitude experimental data points by changing the values of η and ω_0. The values of the dissipation parameter β and the linear frequency ω_0 in (2) were determined by fitting the theoretical curves to the low amplitude experimental data in the figure. This was necessary because the dissipation parameter determined by free decay experiments yielded values too large (by 12%), perhaps as a result of energy lost into the driver after it was

shut off. The theoretical frequency $\omega_0 = (gk)^{1/2}$ yielded values also too large (by 3%), which we discovered was a result of the spilling over of liquid within the viscous penetration distance from the walls. These fitted theoretical curves better represent the properties of the trough and are presented in Figure III.C.4.

The theoretical drive plane showed areas in which we could expect to excite particular modes but we were also interested in the transitions between modes. To show all actual transition boundaries we used the drive plane as a guide and attempted to find all combinations of drive frequency and amplitude at which the given modes could exist. To that end we followed the following rules: first, the drive parameters proper for a pure mode were established; second, we set the amplitude to the desired level; third, we changed the frequency to a value close to the transition region then began varying it in 0.01 Hz increments; finally, each frequency would run for two minutes during which time the transition would occur and the previous frequency was recorded and the next amplitude explored or not and the frequency was varied. With this information plotted in Figure III.C.5 the drive plane could be divided into three areas: one in which no mode could be excited; one in which one of the pure modes of interest could be excited; and one in which both modes could be excited. We called this plot the drive plane and it serves to orient us our explorations.

The experimental data in Figure III.C.5 show agreement with the single-oscillator theory at low drive amplitudes and at frequencies near the linear eigenvalues, but dramatic deviations occur outside these regimes. For low drive amplitud - and for frequencies greater than the linear resonance frequencies, the response amplitude approaches zero uniformly in space, as predicted by the theory. For frequencies less than the linear resonance frequencies but not

inside the Mathieu curve for the lower mode, the response falls to zero uniformly in space from a finite amplitude, also as predicted by the theory. The upward deviations of the experimental data here indicate that some mechanism is closing the tuning curve at response amplitudes smaller than those predicted by the theory. At points inside the Mathieu curve for the lower mode, the upper mode hops to the lower mode by forming a slight kink structure that smoothly evolves as described above.

For drive amplitudes greater than approximately 0.75 mm in Figure III.C.5, there occur two substantial deviations between the theory and experiment. The down-hopping, which occurs along the left set of points, corresponds to kink formation and subsequent self-focusing into the violent state. Along this boundary, greater drive amplitudes cause the average lifetime of the violent state to increase. At high drive levels, the violent state can exist indefinitely. Up-hopping occurs along the right set of points. Between the left and right sets of points, either mode can exist; this is part of the observed hysteresis region for these two parametrically driven modes. As the frequency of the lower mode is slowly increased, note that the up-hopping occurs before the Mathieu curve is reached, where the response is predicted to approach zero. The exception occurs at the bottom of the set of up-hopping points, where the two coincide with the Mathieu curve of the upper mode. This intersection indicates that the counter-traveling wave instability, which leads to up-hopping, is somehow intimately connected with the excitation of the upper mode from rest.

The drive plane plot developed above uses drive parameters to specify a point. In the area where both modes can be excited the response amplitude can be used to differentiate the modes in the trough. To provide a picture of the

response amplitude a plot was made using the two wire probe. This data was taken at a fixed drive amplitude as the frequency was varied from one transition frequency to the next and back. Examination of this plot in Figure III.C.6 shows hysteresis. Deep gravity waves are a softening system and, as the plot shows, the response for the higher mode is greater because it is being driven at a frequency below its resonance frequency. The transitions are shown as discontinuities on the plot because the amplitudes measured are steady state and the transitions occur over a short time.

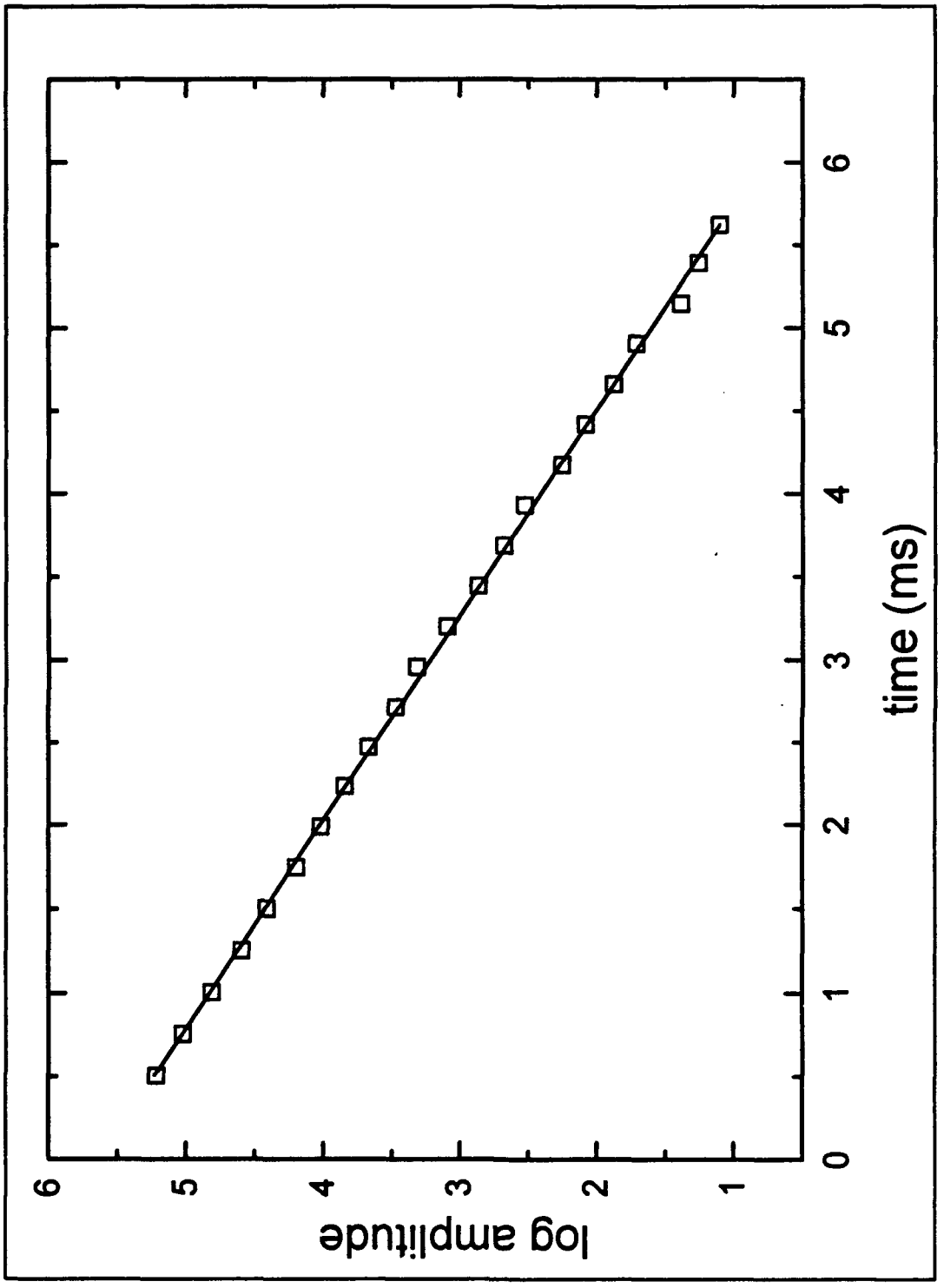

Figure III.C.1. Plot of free decay data for mode 7.

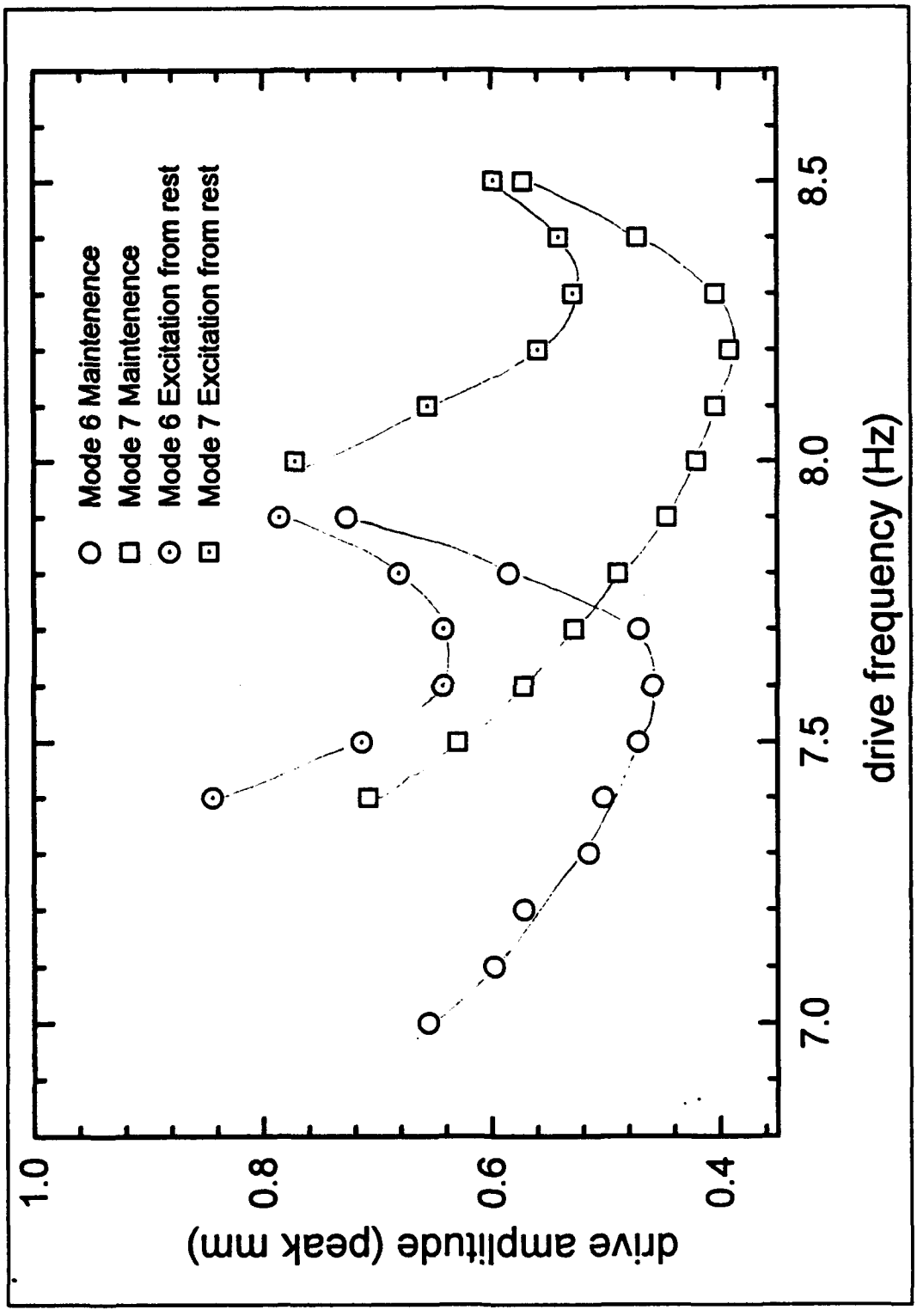

Firgure III.C.2. Experimental drive plane data.

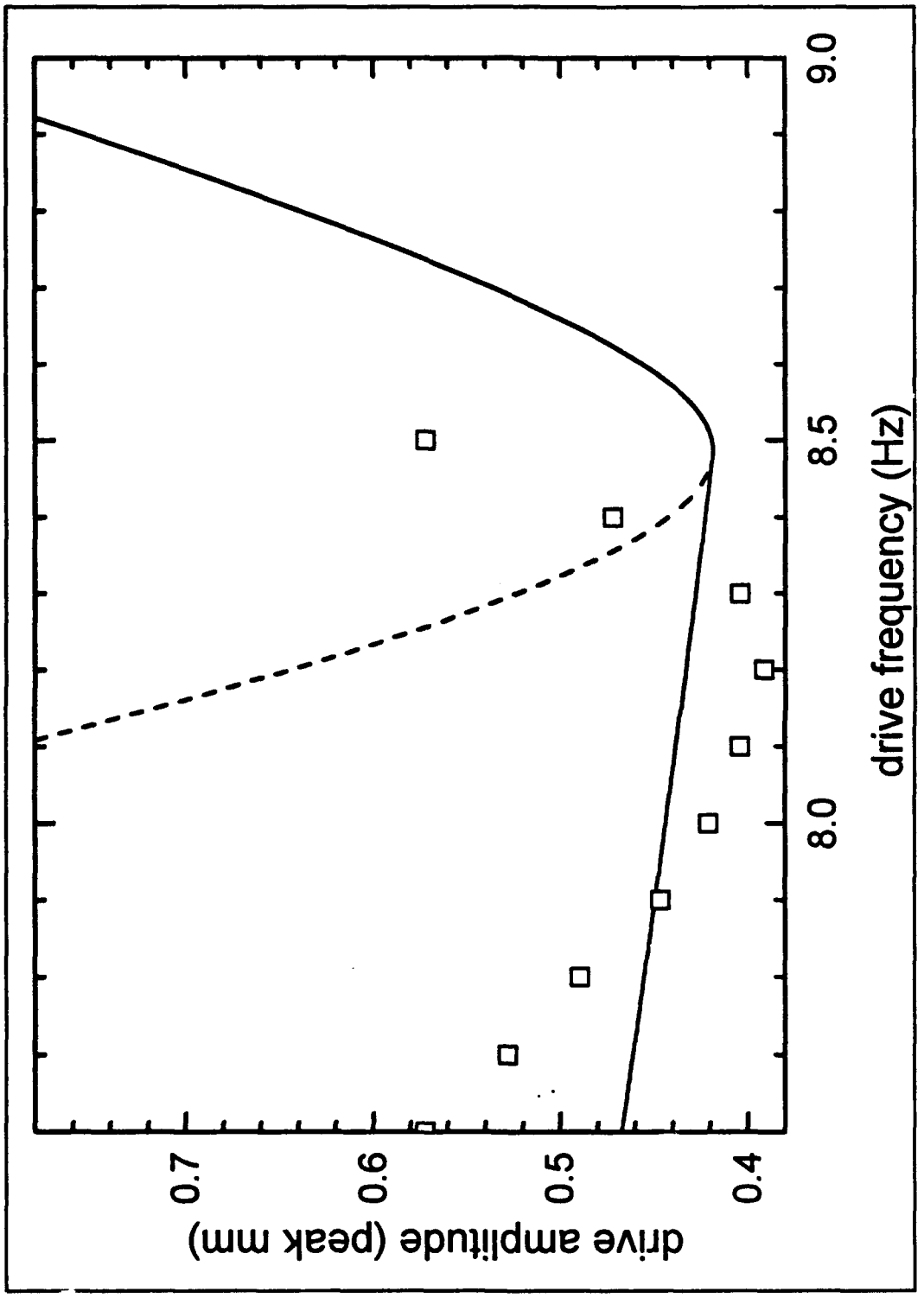

Figure III.C.3. Plot showing the experimental and theoretical drive planes for mode seven.

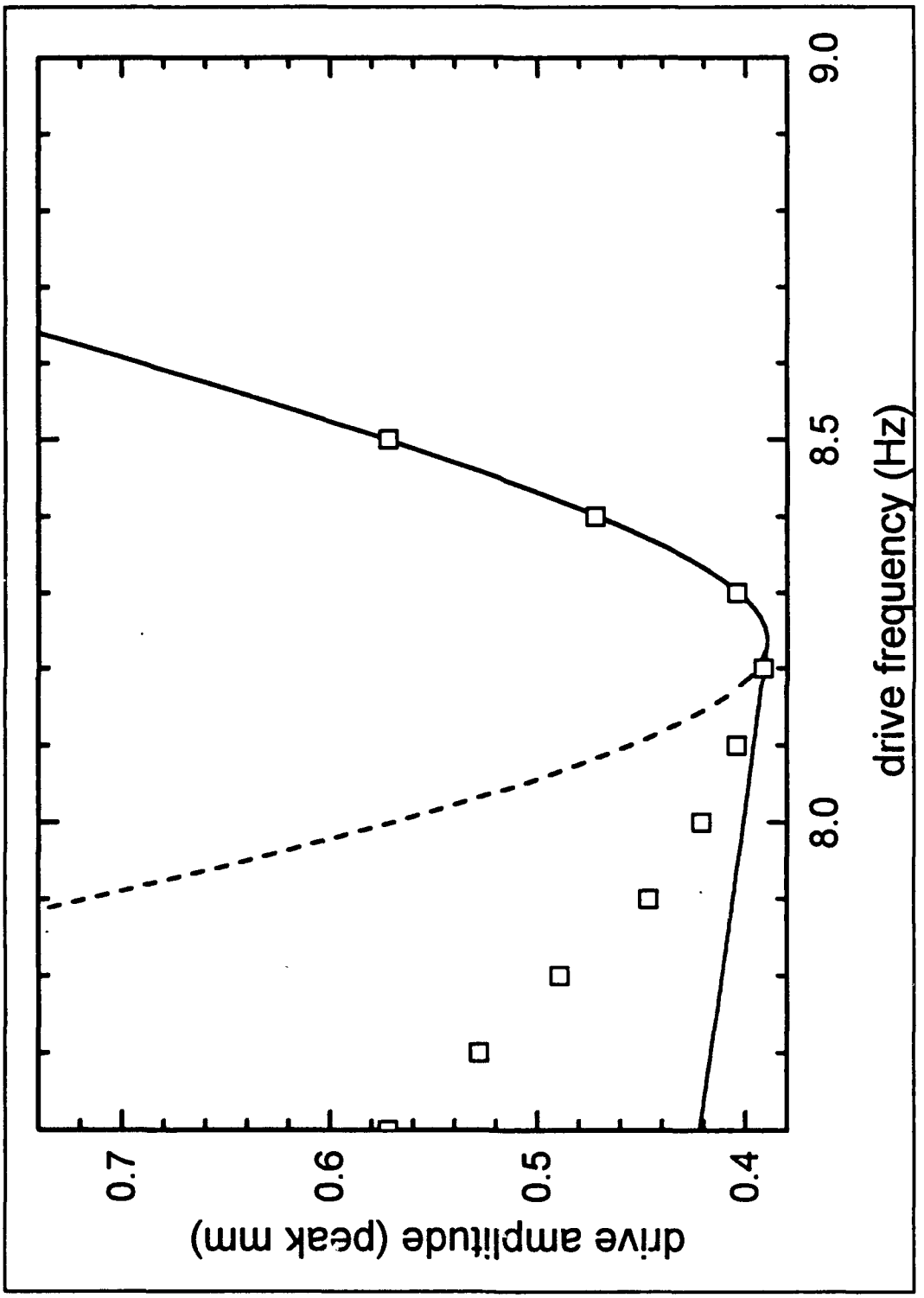

Figure III.C.4. Plot showing theoretical curves fitted to experimental data in Figure III.C.3.

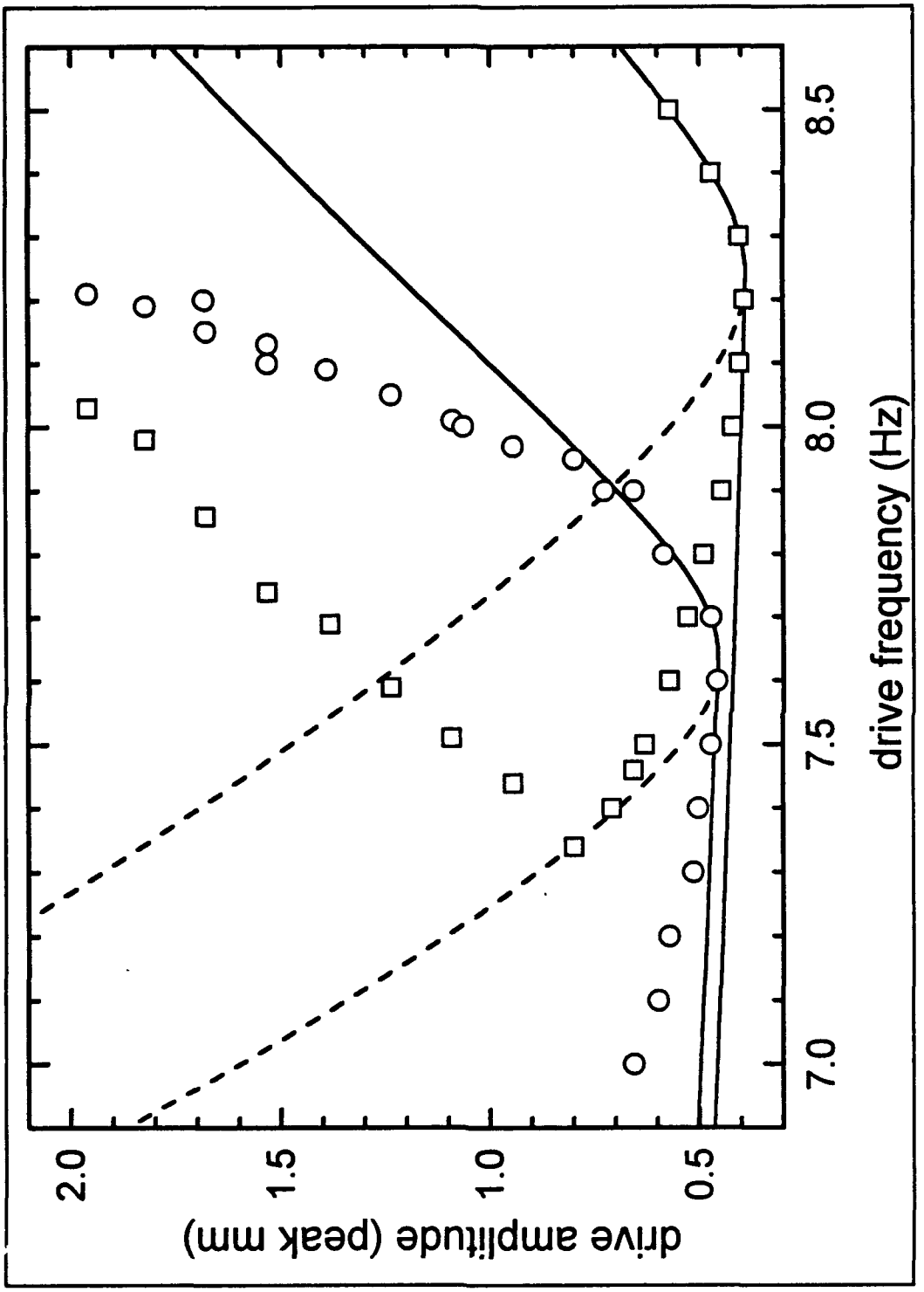

Firgure III.C.5. Plot of the drive plane for modes six and seven.

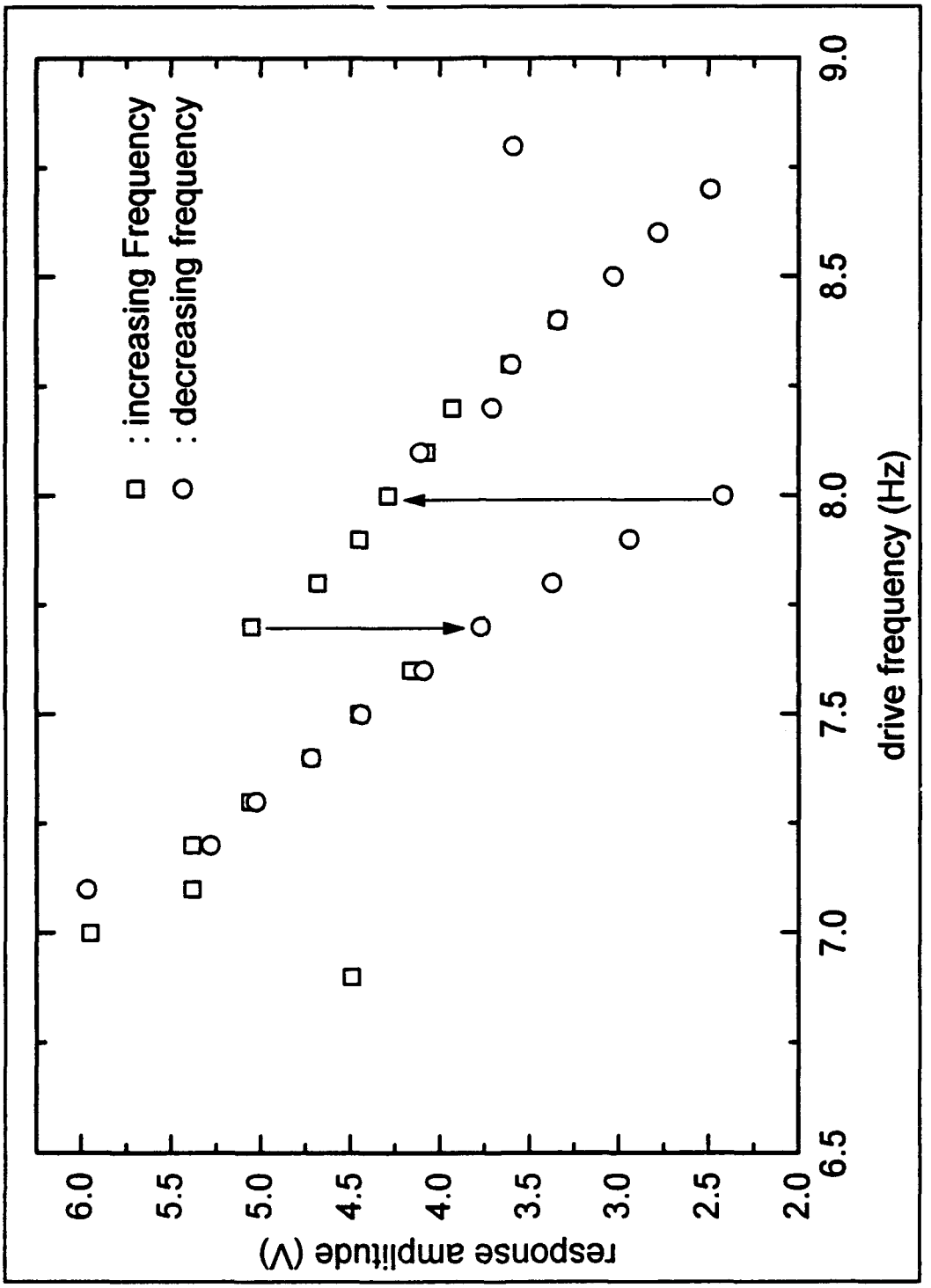

Figure III.C.6. Plot showing the hysteretic response amplitude. The Arrows represent hysteretic jumps.

D. MODE HOPPING

Figure III.D.1 shows a sequence of snapshots of a typical down-hop transition in which the highly focused kink structure persists for only several cycles. The drive frequency and amplitude are constant. Each snapshot was chosen near a turning point of the motion in either the extended mode region or the kink region. The down-hopping transition begins with the formation of a smooth localized kink modulation. This structure is in-phase with extended mode region, but has greater amplitude and smaller wavelength. In the next stage of the transition, the amplitude of the central peak of the kink increases, the wavelength decreases, and the kink occupies a smaller length along the resonator. For intermediate and high drive levels (as quantified below), the central peak ultimately breaks or jets, which causes the amplitude of the peak to drop momentarily to nearly zero. The amplitude then grows with a phase 90^{o} ahead of the extended mode region. For lower drive levels, there is no jetting or breaking; the phase smoothly attains the 90^{o} advance. At this time in the transition, the phase evolves in one of two ways. For high drive levels, the phase can decrease to zero, which leads to a repetition of the breaking or jetting. This is the violent kink structure described above. Depending upon the drive parameters, and also upon chance, the breaking and jetting has been observed to occur for any number of repetitions (from one to at least 10^{4}). For low to intermediate drive levels, or at the conclusion of the violent kink state, the phase increases rapidly from 90^{o} to 180^{o}. As this occurs, one wavelength disappears in the kink region, causing this region to have smaller amplitude and greater wavelength than the extended mode region. The response then relaxes to the uniform state corresponding to this mode.

In summary, the transformation from one mode to the mode with one less wavelength is achieved by the initial formation of a smooth bright kink structure, and then a 180^{o} advance in phase of the central peak which causes the loss of one wavelength. The observations of the down-hop transition suggest that the analytical solution of the surface gravity wave kink corresponds to the smooth kink in the first stage of the transition, and that this structure is subject to a self-focusing instability. It is remarkable that it is possible to maintain the resultant violent kink indefinitely, and it is doubtful whether any analytical treatment can successfully describe this behavior.

Figure III.D.2 shows a sequence of snapshots of a typical up-hop transition. The drive amplitude and frequency are constant, and each snapshot was chosen near a turning point of the motion in the extended mode region. The transition begins with the development of traveling waves in one region. These are superimposed on the standing wave motion, and are counter-traveling toward a central focal point. The amplitude in the region is smaller than the amplitude in the extended mode region, and the phase at the focal point *lags* the phase in the extended mode region. The traveling wave components slowly become stronger, the lag increases to 90^{o}, and the amplitude decreases in this region. The amount of traveling wave motion then relatively quickly decreases and the phase passes from 90^{o} to nearly 180^{o}. As this occurs, an additional wavelength appears in the region, and the amplitude grows such that a smooth bright kink forms. The motion then becomes in-phase with the extended mode region, and the response quickly relaxes to the final uniform state of the new mode.

In summary, the up-hop transition is initialized by counter-traveling wave components that cause the phase at the focal point to lag the phase in the extended mode region. The lag eventually reaches 180^{o}, causing the creation of one wavelength. Our interpretation of the observations is that, whereas a smooth bright kink is responsible for initializing the down-hop transitions, this kink is responsible for finalizing the up-hop transitions. Although this suggests that one transition is simply the time-reversed motion of the other (i.e., that the transitions have an underlying hamiltonian description), some of the behavior appears to violate this picture. Indeed, the counter-traveling wave stage which initiates the up-hopping is not apparent in the finalization of the down-hopping. Furthermore, the kink structure that finalizes the up-hopping only persists for several cycles, and does not exhibit any tendency to self-focus into the violent kink state. This suggests that the up-hop motion approaches but does not attain the unstable kink solution.

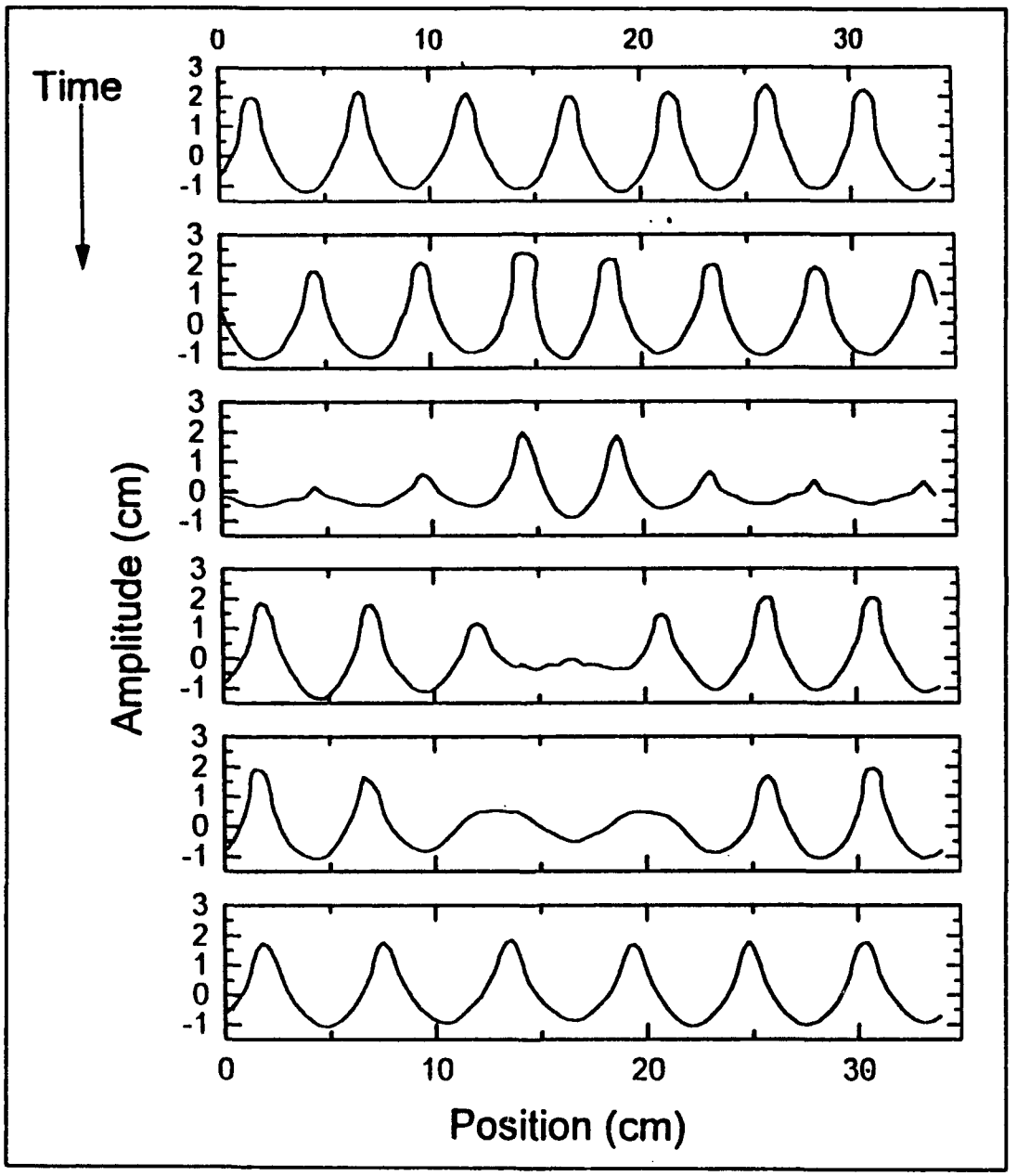

Figure III.D.1. Down hopping sequence for a displacement amplitude of 1.0mm.

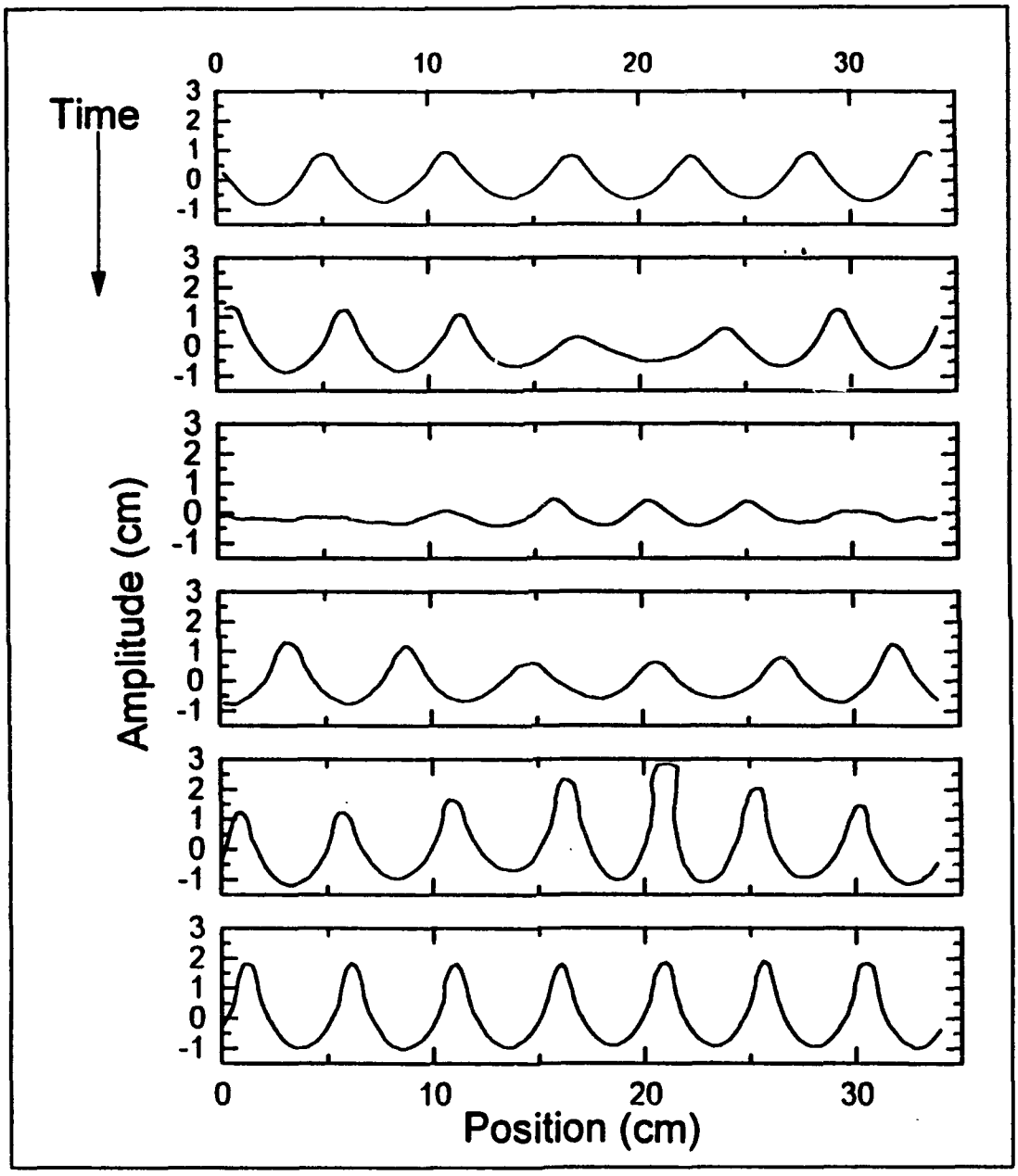

Figure III.D.2. Up hopping sequence for a displacement amplitude of 1.2mm.

IV. CONCLUSIONS AND FUTURE WORK

A. CONCLUSIONS

We have made the first observations of kinks in a non-cutoff standing wave mode in a continuous system. Our particular system involved surface gravity waves in a parametrically driven annular channel of deep liquid, but similar kinks are expected to occur in a variety of systems. We confirmed the theoretical prediction that small amplitude steady state kinks cannot exist. Indeed for a kink to exist many cycles or indefinitely, we found that it must have such a large amplitude that breaking and jetting occur.

Lower amplitude kinks were observed as transients that participate in the transitions from one mode to a mode with one more wavelength ("up-hopping") or one less wavelength ("down-hopping") as the drive frequency is slowly changed. The *creation or destruction of the wavelength* occurs in the kink region. The up-hopping and down-hopping processes do not appear to be essentially the same process time-reversed. This supports the claim that the mode hopping is a far off equilibrium phenomenon.

At lower drive levels, we found that the transitions from one mode to another behaved in accordance with a simple theory. In this case there is no hopping; the modes are separated by frequency intervals in which there is no response.

B. FUTURE WORK

As predicted by theory, the surface wave kink (Fig. I.3) is *bright*; i.e., it has positive energy relative to the background wave. In contrast, a kink in a wave on a string is predicted to be dark. To simulate this situation on a computer, we considered the following model equation of a damped parametrically driven string:

$$y_{tt} + \beta y_t - c^2[1 + \eta\cos(2\omega t)]y_{xx} = \alpha y^3, \qquad \text{(IV.B.1)}$$

where y is the displacement from equilibrium, β is the damping parameter, c is the linear wave speed, η is the drive amplitude, $2\omega t$ is the drive frequency, and where the nonlinear coefficient α must be negative for the system to be stable. The subscripts denote partial differentiation with respect to time t or position x. In our simulations of this equation, we have indeed observed a dark kink during the mode hopping (Fig. IV.B.1).

One area of possible future work is to continue these numerical investigations of mode hopping. The ability to readily obtain clean information on a variety of systems can be very helpful in an overall understanding of the phenomenon.

Our theoretical pursuits have employed the approach of amplitude and wave number modulation of standing waves. Although this theory predicts the existence of surface wave kinks roughly similar to what we observed, the theory suffers from inconsistencies in the perturbation analysis. We are currently developing a nonlinear theory based on waves that propagate in opposite directions. This theory appears to be simpler and more transparent than the previous one. This investigation should be continued with two immediate goals:

a linear stability analysis of finite-amplitude modes in an annular channel, and determining the possibility of a solution corresponding to a kink in a mode. Both of these theoretical directions aim at uncovering the basic mechanism for the hopping instability. Armed with an understanding of this, one can then consider mode hopping and its possible suppression in diode lasers.

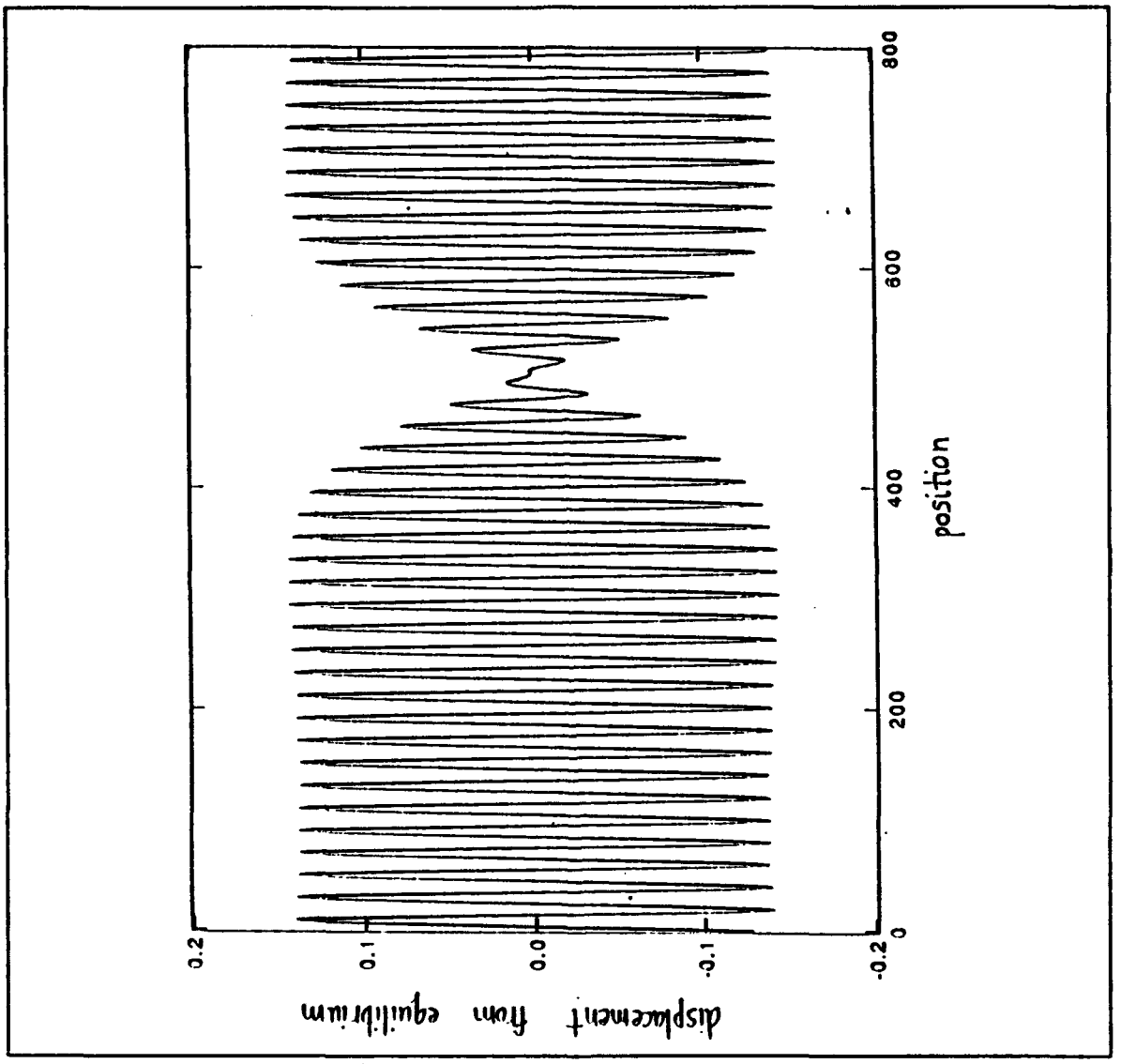

Figure IV.B.1. "Snapshot" of the displacement of a simulated string during the hopping from mode 40 to mode 39. The boundary conditions are periodic. The values of the parameters in (IV.B.1) are $\beta = 0.05$, $c^2 = 1.0$, $\alpha = -1.0$, $\omega = 0.31$, and $\eta = 0.39$.

REFERENCES

A. Davydov, 1985: *Solitons in Molecular Systems* (Reidel, Boston).

B. Denardo, W. Wright, S. Putterman, and A. Larraza, 1990: "Observation of a kink soliton on the surface of a liquid," Phys. Rev. Lett. **64**, 1518-1521.

B. Denardo, B. Galvin, A. Greenfield, A. Larraza, S. Putterman, and W. Wright, 1992a: "Observations of localized structures in nonlinear lattices: Domain walls and kinks," Phys. Rev. Lett. **68**, 1730-1733.

B. Denardo, A. Larraza, S. Putterman, and P. Roberts, 1992b: "Nonlinear theory of localized standing waves, "submitted to Phys. Rev. Lett.

A. Larraza and S. J. Putterman, 1984: "Theory of nonpropagating surface wave solitons," J. Fluid Mech. **148**, 443-449.

J. C. Luke, 1967: " A variational principle for a fluid with a free surface, " J. Fluid Mech. **27**, 375-397.

L. F. Mollenauer, J. P. Gordon, and S. G. Evangelides, 1991: "Multigigabit soliton transmissions traverse ultralong distances," *Laser Focus World*, November, 159-170.

E. Weidel and K. Petermann, 1981: Technical Digest, 3rd Int. Conf., IOOC, San Francisco.

G. B. Whitham, 1965: "A general approach to linear and nonlinear dispersive waves using a Lagrangian, " J. Fluid Mech. **22**, 273-283.

J. Wu, R. Keolian, and I. Rudnick, 1984: "Observation of a nonpropagating hydrodynamic soliton," Phys. Rev. Lett. **52**, 1421-1424.

APPENDIX A. MATHCAD WORKSHEET

Read data file with raw pixel coordinates:

$I := READPRN(n67v3s5)$ $n := rows(I) - 2$ $j := 0..1$

Read the center point, the first element in the data set, and correct for paaralax error:

$I_{0,0} = 326$ $I_{0,1} = 232$ $I_{0,0} := 315$ $I_{0,1} := 233$

Assign the points to cartesian vectors with the center defined as the origin:

$i := 0..n$

$x_i := I_{i+1,0} - I_{0,0}$ $y_i := I_{i+1,1} - I_{0,1}$

Convert to Polar Coordinates:

$i := 0..n$ $r_i := \sqrt{(x_i)^2 + (y_i)^2}$ $\theta_i := angle(x_i, y_i)$

Plot in polar coordinates:

$x_i := r_i \cdot \cos(\theta_i)$ $y_i := r_i \cdot \sin(\theta_i)$

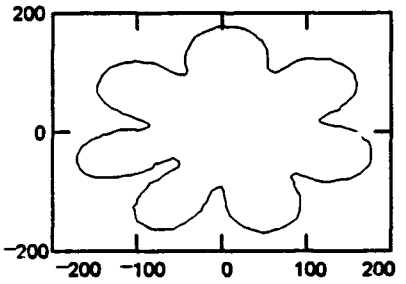

R is assigned from a frame grabbed image of the equilibrium free surface.

$R := 151.753$

Plot in true coordinates:

$x_i := R \cdot \theta_i$ $y_i := R - r_i$ $O := 0$

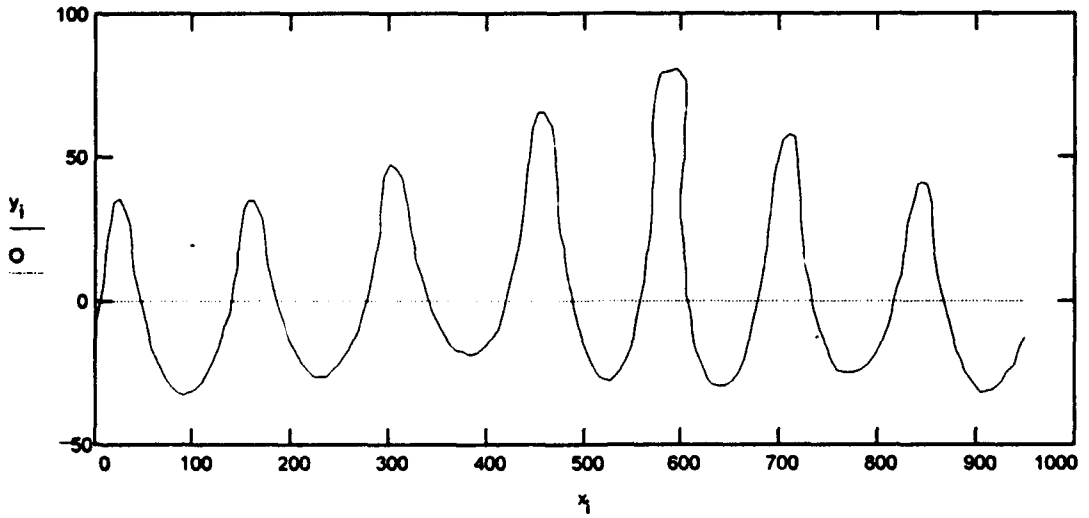

Output the data to a file for importation into our presentation graphics package, Origin 2.0:

$OUTPUT_{i,0} := x_i$ $OUTPUT_{i,1} := y_i$ $WRITEPRN(N67V9S5R) := OUTPUT$

INITIAL DISTRIBUTION LIST

1.	Defense Technical Information Center Cameron Station Alexandria, Virginia 22304-6145	2
2.	Library, Code 52 Naval Postgraduate School Monterey, California 93943-5002	2
3.	Commandant of the Marine Corps Code TE 06 Headquarters, U.S. Marine Corps Washington, D.C. 20380-0001	1
4.	Professor Bruce Denardo Physics Department, Code PH/De Naval Postgraduate School Monterey, California 93943-5002	3
5.	Professor Andrés Larraza Physics Department, Code PH/La Naval Postgraduate School Monterey, California 93943-5002	2
6.	Professor Karlheinz Woehler, Chairman Physics Department, Code PH Naval Postgraduate School Monterey, California 93943-5002	1
7.	Professor Seth Putterman Department of Physics University of California Los Angeles, California 90024-1547	1
7.	Captain Charles B. McClelland, USMC 18 Salt Spray Ln. Cape Elizabeth, Maine 04107	3